



1 Diverging trends in aerosol sulfate and nitrate measured in the remote North Atlantic on
2 Barbados are attributed to clean air policies, African smoke, and anthropogenic emissions

3 Cassandra J. Gaston^{1*}; Joseph M. Prospero¹; Kristen Foley²; Havalá O.T. Pye²; Lillian
4 Custals¹; Edmund Blades¹; Peter Sealy¹; James A. Christie¹

5 ¹Rosenstiel School of Marine, Atmospheric, and Earth Science, University of Miami, Miami,
6 FL 33149, USA

7 ²Office of Research and Development, U.S. Environmental Protection Agency, Research
8 Triangle Park, North Carolina, USA

9 *Correspondence to: cgaston@miami.edu; Ph: 305-421-4979

10



11 **ABSTRACT**

12 Sulfate and nitrate aerosols degrade air quality, modulate radiative forcing and the hydrological
13 cycle, and affect critical biogeochemical cycles, yet their global cycles are poorly understood.
14 To address this issue, we examined trends in 21 years of aerosol measurements made at Ragged
15 Point, Barbados—the easternmost promontory on the island located in the eastern Caribbean
16 Basin. Though the site has historically been used to characterize African dust transport, here
17 we focused on changes in nitrate and non-sea salt (nss) sulfate aerosol from 1990-2011. Nitrate
18 aerosol concentrations are stable at $0.59 \text{ ug/m}^3 \pm 0.04 \text{ ug/m}^3$. Elevated nitrate concentrations
19 in the spring of 2010 as well as during the summer and fall of 2008 are due to transported
20 biomass burning emissions from both northern and southern Africa to our site. In contrast, nss-
21 sulfate decreased 30% at a rate of $0.02 \text{ ug/m}^3/\text{yr}$ in the 1990s, which we attribute to air quality
22 policies enacted in the U.S. and Europe. Starting in 2000, sulfate began to increase to pre-
23 1990s levels of 0.90 ug/m^3 . We used the Community Multiscale Air Quality (CMAQ) model
24 simulations from the EPA's Air QUALity TimE Series (EQUATES) to better understand the
25 changes in nss-sulfate after 2000. The model simulations estimate that increases in
26 anthropogenic emissions, likely from Northern Africa, and increased oxidation efficiency of
27 sulfur dioxide (SO_2) explain the increase in nss-sulfate observed in Barbados. Our results serve
28 as an incentive to better constrain emissions from developing countries and their impact on
29 aerosol burdens in remote regions.

30



31 1. INTRODUCTION

32 Sulfate and nitrate aerosol, formed from gaseous sulfur dioxide (SO_2) and nitrogen oxides (e.g.,
33 $\text{NO}_x \equiv \text{NO} + \text{NO}_2$) as well as reactive nitrogen (e.g., NO_y), contribute to aerosol direct and indirect
34 radiative forcing, impact biogeochemical cycles (Jickells et al., 2017), and degrade air quality
35 (Adams et al., 1999; Appel et al., 1978; Charlson et al., 1992; Lelieveld & Heintzenberg, 1992;
36 Murphy et al., 2006). An outstanding question is, how have sulfate and nitrate aerosol burdens in
37 remote regions changed in response to air quality policies, economic growth, and changing
38 frequency of wildfires—all of which have affected SO_2 and NO_x emissions? Answering this
39 question is important as remote regions are an important barometer of changing global emission
40 inventories, contain ecosystems sensitive to changing chemical inputs (Galloway et al., 2008;
41 Mahowald et al., 2017), and are most sensitive to fluctuations in aerosol burdens that alter aerosol-
42 cloud interactions (Carslaw et al., 2013). Long-term measurement records in remote regions can
43 provide insight into this question as well as further advance current chemical transport and global
44 climate models. However, there are few long-term measurement records in remote regions. In this
45 work, we leverage 21 years of nitrate and sulfate aerosol concentrations measured at Ragged Point,
46 Barbados, a remote site in the eastern North Atlantic marine boundary layer, and use simulations
47 from a hemispheric chemical transport model—the Community Multiscale Air Quality (CMAQ)
48 model within the EPA’s Air QUALity Time Series (EQUATES) (Foley et al., 2023)—to link our
49 observed changes in nitrate and sulfate to changing emissions inventories and meteorological
50 conditions. In turn, comparing the EQUATES model output to our time series provides guidance
51 on which emissions inventories are lacking in in-situ measurements that would improve
52 measurement-model agreement.

53 Ragged Point, Barbados provides a unique opportunity to understand changes in the nitrate
54 and sulfate aerosol burden in the remote North Atlantic marine boundary layer. Aerosol sampling
55 began in 1971 and continues to this day generating an over 50 year measurement record—the
56 longest modern speciated aerosol record to the best of our knowledge (Prospero et al., 2021;
57 Prospero & Mayol-Bracero, 2013). The site serves as a lynchpin for understanding the impact of
58 long-range aerosol transport on the remote North Atlantic marine boundary layer and Caribbean.
59 The site’s primary objective has been to understand the factors affecting the long-range transport
60 of African dust to the Caribbean and North America, which peaks in boreal summer in association
61 with the seasonal northward shift in the intertropical convergence zone (ITCZ). Summer dust
62 events are caused by the strong heating of North Africa, which causes hot, dry dust-laden desert
63 air to be carried to high altitudes, e.g., 4 – 6 km. African Easterly Waves propagate dust westward
64 within an elevated air layer known as the Saharan Air Layer (SAL) that overrides the cool, moist
65 marine boundary layer (Adams et al., 2012; Carlson & Prospero, 1972; Goudie & Middleton, 2001;
66 Tsamalis et al., 2013). Along with dust, anthropogenic emissions from Europe (Lelieveld et al.,
67 2002), North America, and North Africa are also transported to Barbados (Savoie, et al., 2002).

68 Anthropogenic emissions of SO_2 and NO_x from the regions that affect Ragged Point have
69 changed in recent decades due to the opposing effects of decreasing emissions mandated by
70 national air quality policies in developed countries and increasing emissions linked to rapid
71 economic growth in developing countries. The United States (U.S.) curbed emissions of NO_x and



72 SO₂ by passing the Clean Air Act (amended in 1990), resulting in a 92% reduction in SO₂ and a
73 71% reduction in NO_x emissions from 1990-2022 (Aas et al., 2019; Hand et al., 2012;
74 <https://gispub.epa.gov/air/trendsreport/2023/>; Smith et al., 2011; Zhao et al., 2017). European
75 countries passed similar policies resulting in analogous reductions (Aas et al., 2019; Rafaj et al.,
76 2015; Smith et al., 2011; Yang et al., 2020). Notably, reductions in SO₂ can reduce aerosol acidity
77 resulting in increased nitrate aerosol. Further, reductions in pollutant gases can relieve oxidant
78 limitations leading to more efficient oxidation and, therefore, reductions in SO₂ and NO_x may not
79 reduce sulfate and nitrate aerosol as much as expected (Shah et al., 2018). In contrast to clean air
80 policies enacted in the US and EU, emissions in regions such as the Middle East, India, and Africa
81 are continuing to increase due to rapid economic growth with emissions from India predicted to
82 overtake China as the world's largest emitter of SO₂ (Lelieveld et al., 2009; Li et al., 2017;
83 McDuffie et al., 2020). Due to a lack of in situ measurements in many of these regions, chemical
84 transport and emissions inventory models combined with remote sensing have been key tools to
85 understand changing pollutants.

86 In addition to fossil fuel emissions, biomass burning is also a major source of SO₂ and NO_x
87 that can impact the Atlantic (Andreae, 2019; Andreae & Merlet, 2001; Rickly et al., 2022; Roberts
88 et al., 2009; Zuidema et al., 2018). Wildfire activity has a distinct seasonality linked to the dry
89 seasons in Africa. Burning is most intense in the sub-Saharan regions in Northern Africa from
90 November through May while from May through October, the savannah regions in Southern
91 Africa are the most active fire sources (Giglio et al., 2006; Roberts et al., 2009; Van der Werf et
92 al., 2003). African smoke can be transported to Barbados from North Africa in winter and spring
93 (Quinn et al., 2022; Royer et al., 2023; Wex et al., 2016) and, less frequently, from Southern Africa
94 in fall (Trapp et al., 2010). Conditions thought to be related to African climate (e.g., the North
95 Atlantic Oscillation and the position of the Azores High) can cause large quantities of North
96 African dust (and smoke) to be transported during the winter and spring (Chiapello et al., 2005;
97 Doherty et al., 2008, 2012) when dust is also carried to northeastern South America (Barkley et
98 al., 2019; Prospero et al., 1981, 2014).

99 Here we highlight different trends in nitrate and sulfate aerosol over the remote North Atlantic
100 marine boundary layer and relate them to changing emissions. We then compare our observations
101 to simulated concentrations of nitrate and sulfate aerosol using the CMAQ model from EQUATES,
102 which was chosen due to its skill at modeling changes in nitrate and sulfate chemistry within the
103 U.S. (Benish et al., 2022) as well as its ability to simulate constituents and sources of air pollution
104 in remote regions, such as Dhaka, Bangladesh (Golam Sarwar et al., 2023). Our results highlight
105 the importance of long-term atmospheric observations to understand the net outcome of changing
106 global SO₂ and NO_x emissions on both the aerosol burden as well as air quality in distant
107 populations.

108

109 2. METHODS

110 **2.1 Aerosol Collection at the Barbados Atmospheric Chemistry Observatory:** Aerosols were
111 collected daily at the University of Miami's Barbados Atmospheric Chemistry Observatory (UM



112 BACO: <https://baco.rsmas.miami.edu/>) located at Ragged Point, Barbados—the easternmost
113 promontory on the east coast of the island (13.16504N, 59.43207W). The site has been operated
114 by UM since 1971, and aerosol data has been used to document the long-range transport of African
115 dust to the Caribbean and the Americas carried by the easterly trade winds as it is the first landmass
116 encountered by African emissions transported across the Atlantic Ocean (Prospero et al., 2021).
117 Since 1989, aerosols have been collected at the top of a 17-m sampling tower that stands atop a
118 30-m bluff (see Fig 1).



119
120 **Figure 1:** Photo of the Barbados Atmospheric Chemistry Observatory (BACO) including the 17-
121 m sampling tower and two shipping container laboratories.

122 A high-volume sampler pulls air at a nominal rate of 0.75 m³/minute across a 20cm x 25cm
123 Whatman-41 filter. Mass collection efficiencies are 90% for sulfate, 95% for nitrate, and 99% for
124 dust (Savoie & Prospero, 1982). Filters are then folded into quarters under a laminar flow hood,
125 placed in a clean Ziploc bag, and periodically shipped to UM for processing. To ensure that local
126 island emissions are not sampled, the sampling pump is only operational when the wind blows
127 directly from the ocean with speeds greater than 1 m/s. A timer is used to record the “run time”,
128 the total amount of time that the sampling pumps are on during the sampling interval between filter
129 changes. Data with a run time less than 10% of the sampling interval are discarded—these data
130 account for less than 10% of all data collected over the record highlighting the steady easterly
131 winds measured at the site year-round. Procedural blanks are collected weekly by placing a
132 Whatman-41 filter in the filter cassette with the sampling pump off for 15 minutes then placing
133 the filter in a clean Ziploc bag; the blank is subsequently processed along with the daily filter
134 samples.



135 This work focuses on aerosol measurements conducted over 1990-2011, a period that overlaps
136 with the implementation of more stringent air quality policies in the U.S. and Europe. Seasonal
137 trends are also shown where winter is represented by December, January, February (DJF); spring
138 is March, April, May (MAM); summer is June, July, August (JJA); fall is September, October,
139 November (SON). African dust peaks annually at BACO in JJA with episodic transport in DJF
140 and MAM in some years (Prospero & Mayol-Bracero, 2013; Quinn et al., 2022; Royer et al., 2023).

141 **2.2 Quantification of Dust and Soluble Ion Mass Concentrations:** A one-quarter filter section
142 is extracted three times with a total volume of 20 mL of Milli-Q water to remove soluble material.
143 The extracted filter is placed in a combustion oven (500°C) overnight. The resulting ash is weighed
144 ($m_{filter\ ash}$) and corrected for ash present from performing the same technique on the procedural
145 blank ($m_{procedural\ blank}$). The gross ash weight is adjusted by a factor of 1.3 to account for the
146 volatilization of water and minerals during the combustion process (Equation 1, Prospero, 1999;
147 Zuidema et al., 2019). This corrected ash mass concentration is equated to mineral dust
148 concentrations present on the filter based on previous comparisons between filter ash and
149 concentrations of aluminum, a tracer for mineral dust (Prospero, 1999).

$$150 \quad Dust = (m_{filter\ ash} - m_{procedural\ blank\ ash}) * 1.3 \quad (1)$$

151 The filtrate from the washing process is used to quantify soluble ion concentrations. Anions
152 (e.g., chloride (Cl⁻), nitrate (NO₃⁻), and sulfate (SO₄²⁻)) were measured using ion chromatography
153 (IC). Cations (sodium (Na⁺), potassium (K⁺), and calcium (Ca²⁺)) were measured with a flame
154 photometer after 2004 while flame atomic absorption spectrophotometry was used prior to 2004
155 limiting cation analysis to sodium (Savoie et al., 2002). In addition to total soluble ion
156 concentrations, we also report concentrations of non-sea salt (nss) sulfate, which is a useful tracer
157 of sulfur from marine biogenic and pollution emissions, and nss-potassium, a tracer of biomass
158 burning emissions (Andreae, 1983; Keene et al., 1986). Concentrations of nss-SO₄²⁻ and nss-K⁺
159 are calculated using the following mass-based equations and assuming that Na⁺ is a conservative
160 tracer of sea spray aerosol:

$$161 \quad nss - SO_4^{2-} = [SO_4^{2-}] - (0.2517 * [Na^+]) \quad (2)$$

$$162 \quad nss - K^+ = [K^+] - (0.03595 * [Na^+]) \quad (3)$$

163 **2.3 EQUATES Model Products**

164 EPA's Air QUALity Time Series (EQUATES) Project uses the Community Multiscale Air Quality
165 (CMAQ) model, a 3-D chemical transport air quality model, to simulate air quality over a
166 continuous 2002-2019 time period (Foley et al., 2023). CMAQ accounts for gas, cloud, and aerosol
167 chemistry, including processes such as in-cloud sulfate formation from the oxidation of SO₂.
168 EQUATES uses CMAQv5.3.2 (Appel et al., 2021) to model the Northern Hemisphere using 108-
169 km resolution and 44 vertical layers (Mathur et al., 2017). Meteorological data is predicted using
170 the Weather Research and Forecasting model (WRFv4.1.1). Emissions from outside the
171 contiguous U.S. and China are generated using the Hemispheric Transport of Air Pollution version
172 2 inventory for the year 2010 (HTAPv2.2) and are scaled to other years using the Community
173 Emissions Data System (CEDs) for the years 2002-2019. The Fire INventory from NCAR (FINN)



174 is used to generate biomass burning emissions (Wiedinmyer et al., 2011), lightning NO_x emissions
175 are derived from the Global Emissions IniAtive (GEIA), biogenic volatile organic compounds
176 (VOCs) are from MEGAN2, and soil NO_x is from CAMSv2.1.

177 In this study, EQUATES was used to better understand observed trends, namely in nss-sulfate,
178 post 2000 when concentrations unexpectedly increased. The model product is not available for the
179 years prior to 2000. The analysis focused on dust, sea spray, nitrate, sulfate, and gaseous SO₂ and
180 NO₂. In addition to anthropogenic sources of SO₂, natural sources such as dimethyl sulfide (DMS)
181 were included in model runs. Species predictions were extracted from the lowest CMAQ model
182 layer (~10m in thickness) for a receptor area over the Atlantic Ocean to the east of the island from
183 59.5627°W to 56.5448°W longitude and 14.3989°N to 11.4566°N latitude (equivalent to 16 grid
184 cells). Simulated concentrations of aerosol sulfate, nitrate, calcium, potassium, and sodium were
185 obtained for fine mode aerosol (e.g., Aitken and accumulation mode) and coarse mode aerosol.
186 Previous studies have shown that most of the aerosol mass at Ragged Point is below 10 μm
187 diameter (Prospero et al., 2001). Because aerosol filters collected at BACO capture total suspended
188 particulate matter, model outputs of fine and coarse mode aerosol concentrations were combined
189 to give total aerosol mass concentrations of sulfate, nitrate, Na⁺, K⁺, and Ca²⁺. Concentrations of
190 nss-sulfate and nss-K⁺ were calculated using Equations 2 and 3, respectively, and model outputs
191 of total Na⁺ mass concentrations, total sulfate mass concentrations, and total K⁺ mass
192 concentrations. We calculated concentrations of nss-Ca²⁺, which has been shown to be a good
193 tracer for mineral dust in Barbados (Savoie & Prospero, 1980), and dust mass concentrations were
194 then calculated using the upper crustal abundance of Ca²⁺ in soil (4.1%) (Taylor & McLennan,
195 1985) as shown in Equations 4 and 5.

$$196 \quad nss - Ca^{2+} = [Ca^{2+}] - (0.0376 * [Na^+]) \quad (4)$$

$$197 \quad Dust = [nss - Ca^{2+}] * 24.1 \quad (5)$$

198 We first assessed the ability of the EQUATES CMAQ simulations to capture trends in different
199 aerosol types observed at Ragged Point. Simulations of dust and sodium from EQUATES capture
200 seasonal and monthly observed trends in dust (see Fig S1 and S2 of the Supporting Information
201 (SI)). However, the model overpredicts sodium (Na⁺, a proxy for sea spray) by a factor of 3-4 (Fig
202 S2) and underpredicts dust by an average factor of ~7. This low bias for dust in CMAQv5.3.2 is
203 consistent with CMAQ development that occurred after the EQUATES simulations were
204 complete. A bugfix to the online dust emissions module in CMAQv5.4 increases dust emissions
205 by a factor of 3-7 over the Sahara Dessert and parts of Asia (see the CMAQv5.4 release notes for
206 further information; <https://www.epa.gov/cmaq/cmaq-documentation#release-notes>).

207 In addition to simulating observed aerosol concentrations, EQUATES was also used to examine
208 trends in gaseous indicators of anthropogenic and biomass burning emissions, oxidant
209 concentrations and oxidant ratios important for investigating changes in the oxidation efficiency
210 of pollutant gases and the subsequent formation of nitrate and sulfate aerosol. Further, EQUATES
211 was used to investigate whether the oxidation efficiency of SO₂(g) changed during the 2002-2011
212 period. The oxidation ratio was calculated from Equation 6 (Shah et al., 2018):



213
$$\text{Oxidation Ratio} = \frac{\text{nss-SO}_4^{2-}}{\text{nss-SO}_4^{2-} + \text{SO}_2} \quad (6)$$

214 For this calculation, we used EQUATES model data for SO₂(g) concentrations and filter-based
215 observations of nss-sulfate.

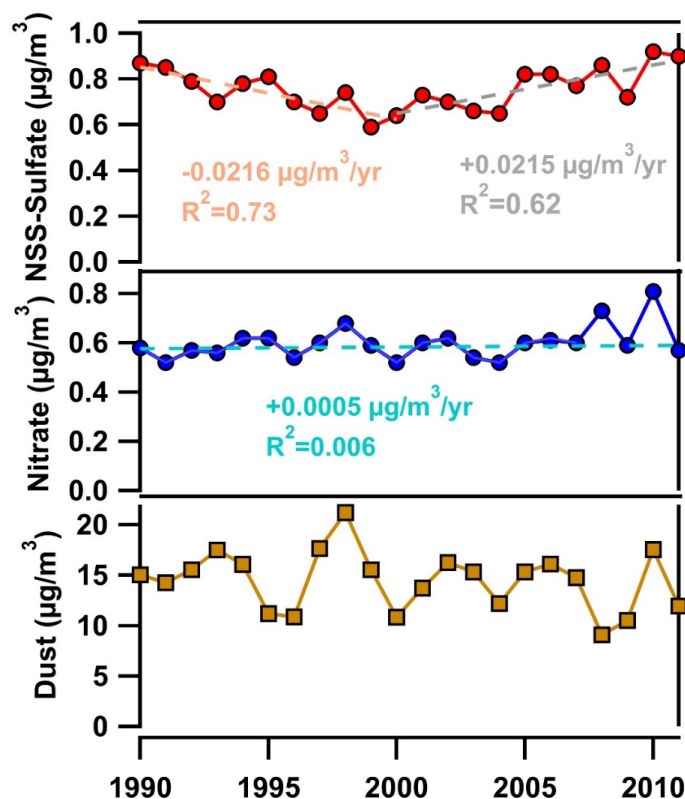
216 **2.4 HYSPLIT Back-trajectory Analysis**

217 Air mass back-trajectory analysis was performed using NOAA's Hybrid Single-Particle
218 Lagrangian Integrated Trajectory (HYSPLIT) model (Draxler & Rolph, 2011; Rolph et al., 2017;
219 Stein et al., 2015). 315-h back-trajectories were initiated at heights of 500, 1000, and 2000-m to
220 capture both SAL and boundary layer transport. Frequency plots were also generated to illustrate
221 seasonal differences in air mass transport and origin. We used global National Center for
222 Environmental Prediction (NCEP) reanalysis data that goes back in time far enough to examine
223 trajectories from our dataset (Kramer et al., 2020). The finer resolution Global Data Assimilation
224 System (GDAS) dataset (1° resolution) was used to examine trends in 2008, 2009, and 2010 when
225 transport conditions strongly impacted nitrate aerosol concentrations.

226 **3. RESULTS**

227 **3.1 Measured Trends from 1990-2011 at Ragged Point: Nitrate has remained constant** 228 **while NSS-Sulfate initially declined then subsequently increased.**

229 Figure 2 shows yearly measured average mass concentrations of non-sea salt (nss) sulfate and
230 nitrate from 1990 through 2011. Nitrate concentrations are remarkably stable from 1990 to 2011
231 ($R^2=0.006$, $p>0.05$ (not significant)) with an average concentration of $0.59 \text{ ug/m}^3 \pm 0.04 \text{ ug/m}^3$.
232 However, two anomalous peaks in nitrate are observed in 2008 and 2010 with annual average
233 nitrate concentrations of 0.73 and 0.81 ug/m^3 , respectively. In contrast, nss-sulfate decreases by
234 30% from an average concentration of 0.84 ug/m^3 starting in 1990 to a minimum of 0.64 ug/m^3 in
235 2000 at a rate of $0.022 \text{ ug/m}^3/\text{yr}$. Subsequently, sulfate gradually increased to 0.91 ug/m^3 in 2010
236 and 0.90 ug/m^3 in 2011, maximums across the entire record. The trends in the yearly average mass
237 concentrations of nitrate and nss-sulfate are significantly different ($p\text{-value} < 0.005$), which can be
238 explained by either different sources or different rates of change for precursor NO_x and SO₂
239 emissions or different responses in aerosol production to changing emissions (Shah et al., 2018;
240 Vasilakos et al., 2018).



241

242 **Figure 2:** Yearly averages of non-sea salt sulfate (NSS Sulfate, red line, top panel), nitrate (middle panel,
243 blue line), and dust (bottom panel, brown line with squares) measured at Ragged Point, Barbados from
244 1990-2011. Dashed lines show changes in NSS Sulfate pre-2000 (orange), post-2000 (gray line) and for
245 nitrate (teal line) without the spikes in 2008 and 2010 considered.
246

247 The Barbados yearly trends differ from long-term observations of aerosol and precipitation
248 chemistry measured at Tudor Hill, a site on the west coast of Bermuda, from 1989-1997 and from
249 2006-2009 as part of the same program as that at Barbados and using the same protocols including
250 sampling only when winds are easterly and over the ocean (Keene et al., 2014; Savoie, et al., 2002).
251 Aerosol nitrate is constant at both sites; however, the nitrate annual mean at Bermuda is ~ 1.05
252 $\mu\text{g}/\text{m}^3$, roughly double the nitrate observed at Ragged Point (Keene et al., 2014; Savoie, et al.,
253 2002) while the decline in nss-sulfate observed in Bermuda from $\sim 2.59 \mu\text{g}/\text{m}^3$ in 1989 to ~ 1.63
254 $\mu\text{g}/\text{m}^3$ in 2009 is also greater than our observations at Ragged Point (Keene et al., 2014).
255 Furthermore, sulfate aerosol in Bermuda declines over the entire record and does not exhibit the
256 same reversal in the 2000s that we observe at Barbados. The difference in concentrations and trend
257 in nss-sulfate observed at Ragged Point compared to that at Bermuda is not entirely surprising
258 given that the Bermuda site is more directly influenced by anthropogenic emissions from the U.S.
259 compared to Barbados, which is a more remote site influenced by a multitude of emission sources
260 (Savoie, et al., 2002).

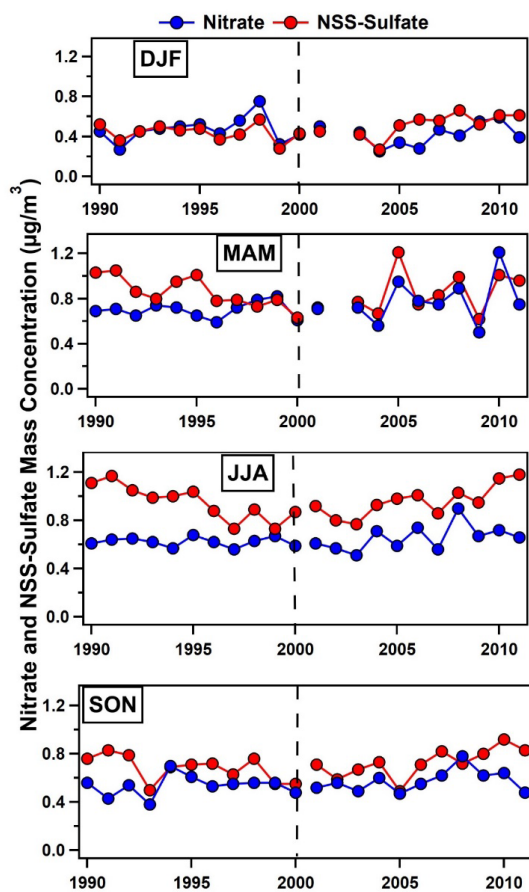


261 To assess whether annual trends in nss-sulfate and nitrate observed in Barbados are associated
262 with African aerosol transport conditions, annual average measured dust mass concentrations are
263 also shown in Fig 2. Annually averaged dust concentrations show no appreciable increase or
264 decrease from 1990-2011. Therefore, nss-sulfate aerosol shows no correlation with African dust
265 mass concentrations. However, nitrate aerosol is modestly correlated with dust ($R^2=0.3$).
266 Comparing seasonal nitrate and dust mass concentrations by year reveals tighter correlations
267 between nitrate and dust for DJF and MAM (0.46 and 0.4, respectively, see Fig S3). DJF and
268 MAM are not the peak dust transport seasons to the Caribbean, but they are the seasons that favor
269 co-transport of dust and biomass burning emissions from Northern Africa (Royer et al., 2023).

270 **3.1.2 Seasonal Patterns in Air Mass Trajectories and Nitrate Concentrations: Transport** 271 **of African biomass burning likely explains elevated nitrate concentrations**

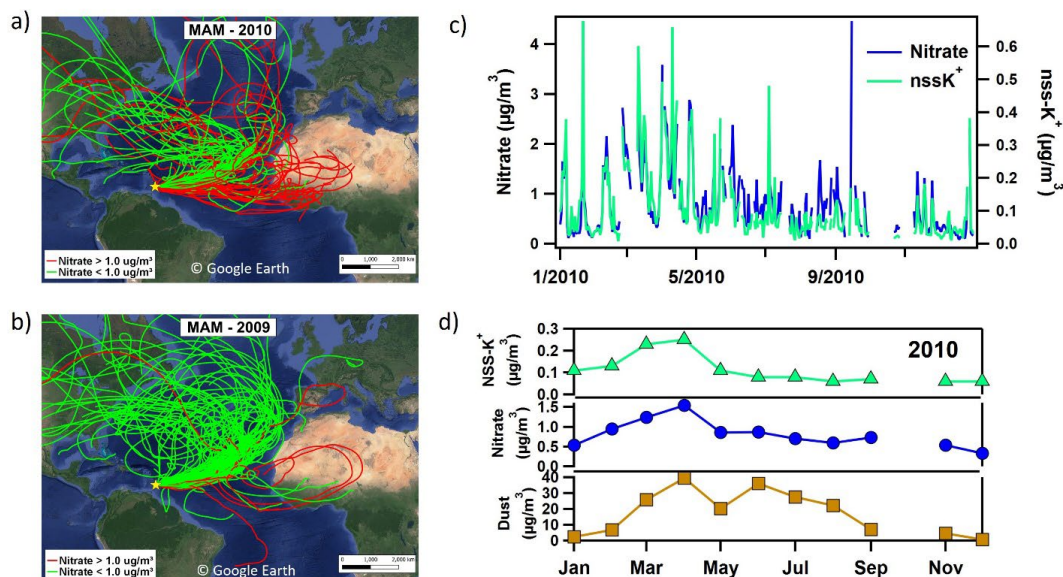
272 HYSPLIT air mass back-trajectories reveal similar seasonal patterns each year with
273 predominantly easterly transport to the site year-round (see Fig S4, which shows representative 5-
274 day air mass back-trajectory frequency plots). DJF has some trajectories that intercept North
275 America and some from the northern part of the Atlantic Ocean toward Europe, MAM trajectories
276 are easterly, JJA trajectories are from the northeast along the coast of Africa, and SON trajectories
277 are from the east with some from the southeast close to the coast of South America.

278 Figure 3 shows trends in nss-sulfate and nitrate during different seasons (e.g., DJF, MAM, JJA,
279 and SON). Increases in nitrate in 2008 are driven by high nitrate concentrations in JJA and SON
280 in 2008, with most of the increase in September, while high nitrate levels in 2010 are primarily
281 observed during MAM. In 2010, a transition from an El Niño to the strongest La Niña event on
282 record occurred (Wolter & Timlin, 2011; Zhang et al., 2019), and long-range transport from Africa
283 was anomalously high during the springtime as evidenced by high mass concentrations of dust in
284 the spring of 2010 (Zuidema et al., 2019). Daily air mass back-trajectories passed more frequently
285 over the African continent in MAM of 2010 compared to MAM of 2009 (26 vs 6 days) (Fig 4a
286 and b), and nitrate levels exceeded 1 ug/m^3 on over half of those days when trajectories traversed
287 the N African continent. Figure 4 focuses on trajectories initiated at 500-m height, and if
288 trajectories initiated at 1000-m are also included, then transport over the N African continent
289 occurs on 36 days in MAM of 2010 or 82% of days when nitrate levels exceeded 1 ug/m^3 .
290 However, during the summertime peak (JJA) in African dust transport in 2010, nitrate does not
291 show the same increase as dust despite frequent transport from N Africa (see Fig 4d). Further, Fig
292 4c and d compares daily and monthly mean concentrations of nitrate, dust, and non-sea salt
293 potassium (e.g., nss- K^+), which is a marker for biomass burning emissions (Andreae & Merlet,
294 2001). Nitrate and nss- K^+ clearly track each other and are both elevated in the spring of 2010.
295 Although biomass burning peaks in December and January while MAM is the tail end of the burn
296 season in North Africa (Giglio et al., 2013; Roberts et al., 2009), the high nitrate loadings observed
297 in 2010 in spring are likely due to strongly favorable transport conditions that transport both dust
298 and smoke to Barbados during this year.



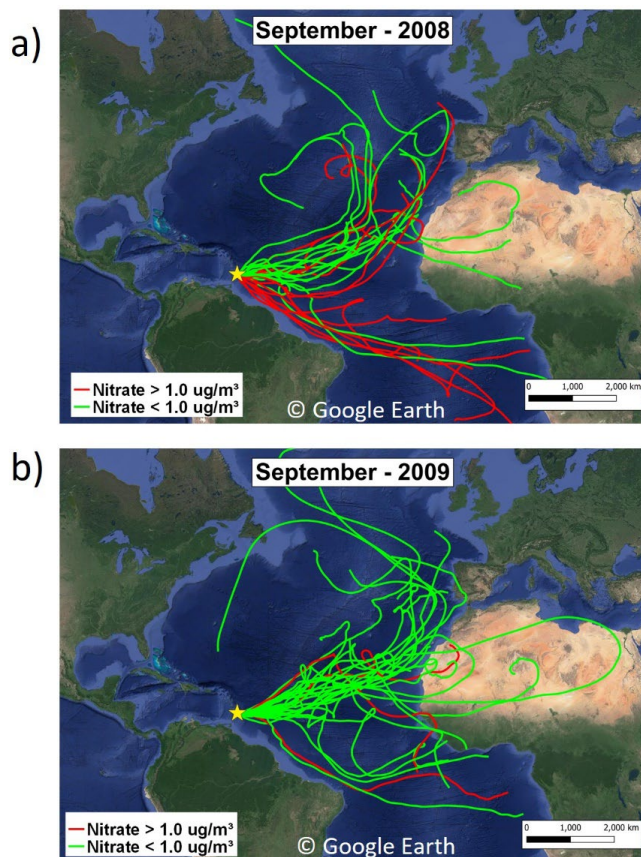
299

300 **Figure 3:** Average yearly concentrations of nitrate (blue markers), and nss-sulfate (red markers) for winter
301 (DJF), spring (MAM), summer (JJA), and fall (SON). The black dashed line denotes the year 2000 when
302 nss-sulfate trends shifted from decreasing to increasing.



303
304 **Figure 4:** 315-h air mass back-trajectories initiated at 500-m for MAM a) 2010 and b) 2009. Back-
305 trajectories labeled in green are for days where nitrate concentrations measured at Ragged Point were < 1
306 $\mu\text{g}/\text{m}^3$ while trajectories labeled in red had nitrate > 1 $\mu\text{g}/\text{m}^3$ (from Google Earth). c) Daily comparison of
307 nitrate and non-sea salt potassium (nss-K^+), a biomass burning marker, show a tight correlation ($R^2=0.62$).
308 d) Monthly average concentrations of dust (brown), nitrate (blue), and nss-K^+ (green) for 2010.

309 Similar to 2010, air mass back-trajectories traversed the African continent on just 40% of the
310 days in JJA but 82% of days in September of 2008 with nitrate concentrations > 1 $\mu\text{g}/\text{m}^3$ (Fig S5
311 and Fig 5a). If trajectories initiated at the 1000-m level are included, then African transport occurs
312 on 64% of days in JJA with nitrate concentrations > 1 $\mu\text{g}/\text{m}^3$. In JJA, most of the air mass back-
313 trajectories pass through the N African continent. However, in September, trajectories take a more
314 southerly route traversing near the South American coast, sub-Saharan Africa, and southern Africa
315 (Fig 5a). Figure 5b shows trajectories for September but in 2009, when fewer trajectories take a
316 southerly route and nitrate concentrations rarely exceed 1 $\mu\text{g}/\text{m}^3$. September is during the peak of
317 the burn season in sub-Saharan and southern Africa and also dovetails with strong smoke transport
318 over the Atlantic Ocean due to the increased intensity of the African Easterly Jet (Adams et al.,
319 2012; Adebisi & Zuidema, 2016; Zuidema et al., 2018). Air mass back-trajectories in September
320 from southern and sub-Saharan Africa to our measurement sites in Barbados and Cayenne have
321 been linked with African smoke transport (Barkley et al., 2019; Trapp et al., 2010) further
322 suggesting a link between elevated concentrations of nitrate measured at Barbados with
323 transported African smoke. Further, biomass burning in the Amazon also peaks in SON (Adams
324 et al., 2012) and could also explain the increase in nitrate in this season in 2008.



325

326 **Figure 5:** 315-h air mass back-trajectories initiated at 500-m for September a) 2008 and b) 2009. Back-
327 trajectories labeled in green are for days where nitrate concentrations measured at Ragged Point were < 1
328 $\mu\text{g}/\text{m}^3$ while trajectories labeled in red had nitrate > 1 $\mu\text{g}/\text{m}^3$ (from Google Earth).

329

330 **3.1.3 Seasonal Patterns in Non-Sea Salt-Sulfate, Impacts of SO₂ Reductions in the US and** 331 **EU, and Possible Impacts from SO₂ Increases in Africa**

332 Figure 3 reveals that the decrease in sulfate and subsequent increase are measured year-round
333 during all seasons. Table 1 further provides correlation coefficients and the rate of change in either
334 nitrate or sulfate in $\mu\text{g m}^{-3}\text{yr}^{-1}$ for data collected pre- and post-2000 when the trend in nss-sulfate
335 changed. Pre-2000, nss-sulfate shows a consistent decline in each season except for winter with
336 the strongest reduction measured in JJA at $-0.037 \mu\text{g m}^{-3}\text{yr}^{-1}$ ($R^2=0.72$, Table 1). Post-2000, nss-
337 sulfate increased during every season except MAM with the highest increases again in JJA at a
338 similar rate to the pre-2000 decline at $+0.030 \mu\text{g m}^{-3}\text{yr}^{-1}$ ($R^2=0.61$, Table 1). In contrast, nitrate
339 shows no trend (e.g., $R^2<0.2$) in any season except a slight increase of $0.015 \mu\text{g m}^{-3}\text{yr}^{-1}$ post-2000
340 in JJA. Unlike nitrate which showed intermittent spikes associated with increased biomass burning

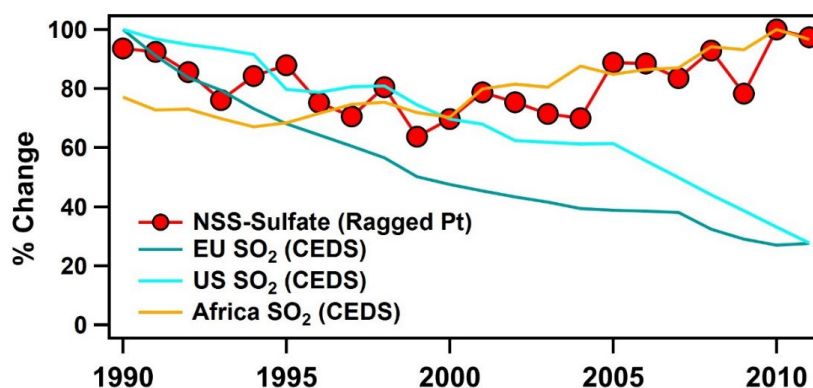


341 aerosol transport periods, the persistent increases in nss-sulfate observed during all seasons more
 342 likely reflect either increased emissions or more efficient oxidation of SO₂.

343 **Table 1:** Seasonal trends in nitrate and nss-sulfate shown pre- and post-2000. The rate of change in ug/m³/yr
 344 is shown and the correlation coefficient is also included. Values of R²<0.2 were denoted as having
 345 “No Trend”. DJF represents winter, MAM represents spring, JJA represents summer, and SON
 346 represents fall.

Season	Compound	Pre-2000 Rate of Change (ug/m ³ /yr)	Post-2000 Rate of Change (ug/m ³ /yr)
DJF	Nitrate	+0.0088 (R ² =0.05, No Trend)	+0.0094 (R ² =0.07, No Trend)
	NSS-Sulfate	-0.0055 (R ² =0.05, No Trend)	+0.025 (R ² =0.48)
MAM	Nitrate	+0.0023 (R ² =0.01, No Trend)	+0.018 (R ² =0.08, No Trend)
	NSS-Sulfate	-0.033 (R ² =0.64)	+0.017 (R ² =0.09, No Trend)
JJA	Nitrate	-0.0015 (R ² =0.02, No Trend)	+0.015 (R ² =0.21)
	NSS-Sulfate	-0.037 (R ² =0.72)	+0.030 (R ² =0.61)
SON	Nitrate	+0.0031 (R ² =0.02, No Trend)	+0.01 (R ² =0.13, No Trend)
	NSS-Sulfate	-0.018 (R ² =0.29)	+0.024 (R ² =0.44)

347
 348
 349 Figure 6 compares yearly trends in Ragged Point nss-sulfate along with SO₂ emissions reported
 350 from the Community Emissions Data System (CEDs) (McDuffie et al., 2020). We focus on the
 351 most likely sources to impact Ragged Point including emissions from the US, EU, and Africa. A
 352 similar figure comparing nitrate concentrations measured at Ragged Point and nitrogen dioxide
 353 (NO₂) emissions from CEDs can be found in the SI (Fig S6). Our near constant nitrate mass
 354 concentrations do not match the decline in NO₂ observed in the EU and US and increase in NO₂
 355 in Africa. In contrast, decreases in nss-sulfate observed from 1990-2000 at Ragged Point closely
 356 follow the 32% and 58% reductions of SO₂ emissions in the U.S. and Europe, respectively (Fig 6)
 357 (Aas et al., 2019; Hand et al., 2012; McDuffie et al., 2020; Rafaj et al., 2015; Yang et al., 2020).
 358 Our finding that changing SO₂ emissions in the EU and US is reflected in our record at Ragged
 359 Point is in agreement with previous work examining both anthropogenic and biogenic sulfate
 360 (Savoie, et al., 2002). Figure 6 also compares the recovery of nss-sulfate observed at Ragged Point
 361 after 2000 to increasing emissions of SO₂ from Africa where emissions of SO₂ increased by 37%
 362 (McDuffie et al., 2020). We next utilized the CMAQ model results from EQUATES to gain further
 363 insight into the observed recovery of nss-sulfate (post-2000) and determine if other factors such as
 364 changes in the oxidation efficiency of SO₂ and meteorological changes and emissions from smoke
 365 or anthropogenic emissions affected our observations.



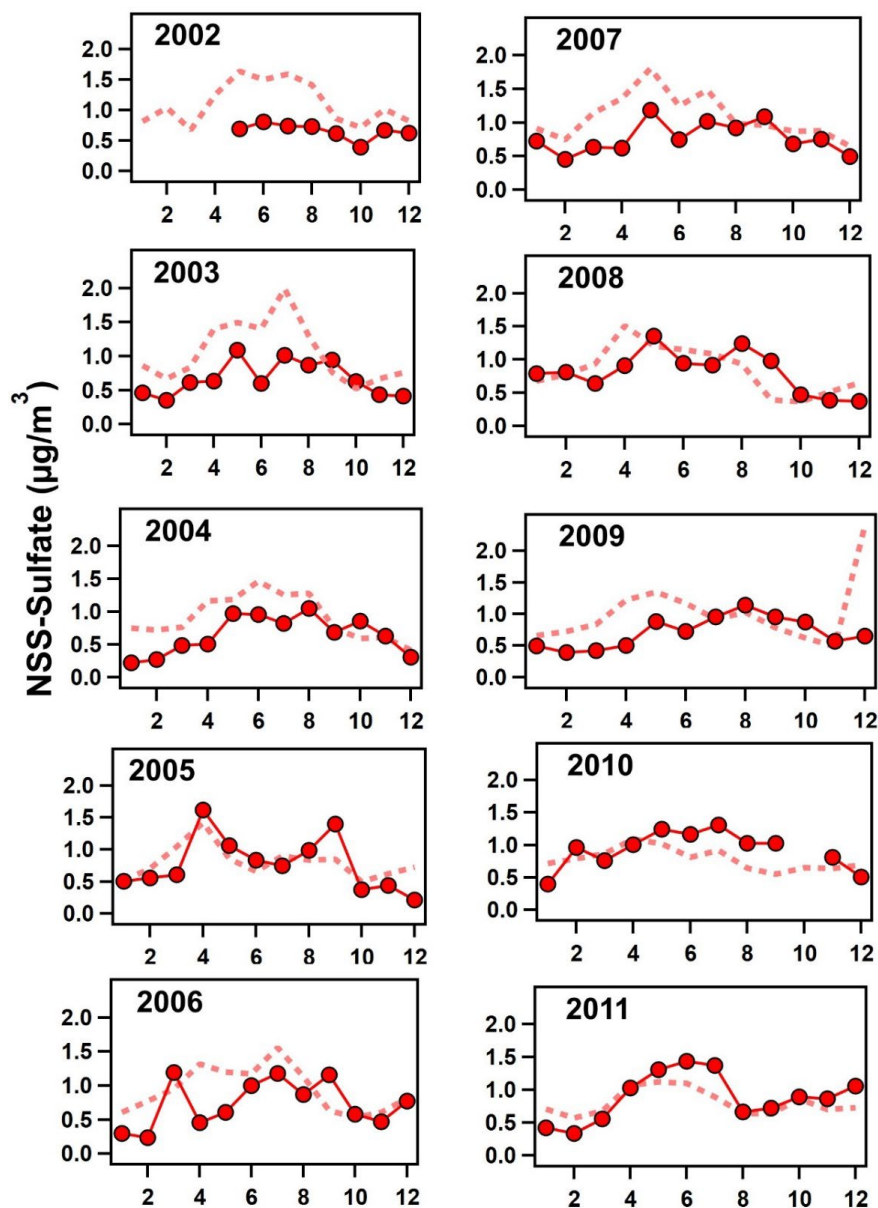
366

367 **Figure 6:** NSS-Sulfate mass concentrations measured at Ragged Point from 1990-2011 are shown in red.
368 NSS-Sulfate mass decreases from 0.87 $\mu\text{g}/\text{m}^3$ in 1990 to 0.64 $\mu\text{g}/\text{m}^3$ in 2000 and increases again to 0.90
369 $\mu\text{g}/\text{m}^3$. Emissions of sulfur dioxide (SO_2) from the CEDs emissions inventory from McDuffie et al., 2020
370 are included for comparison. Decreasing emissions of SO_2 from the US and EU are shown in blue lines.
371 U.S. SO_2 reduces from 21.12 to 5.85 Tg S/yr and EU SO_2 reduces from 28.06 to 7.74 Tg S/yr. SO_2 emissions
372 from Africa increase from 4.13 to 5.95 Tg S/yr.

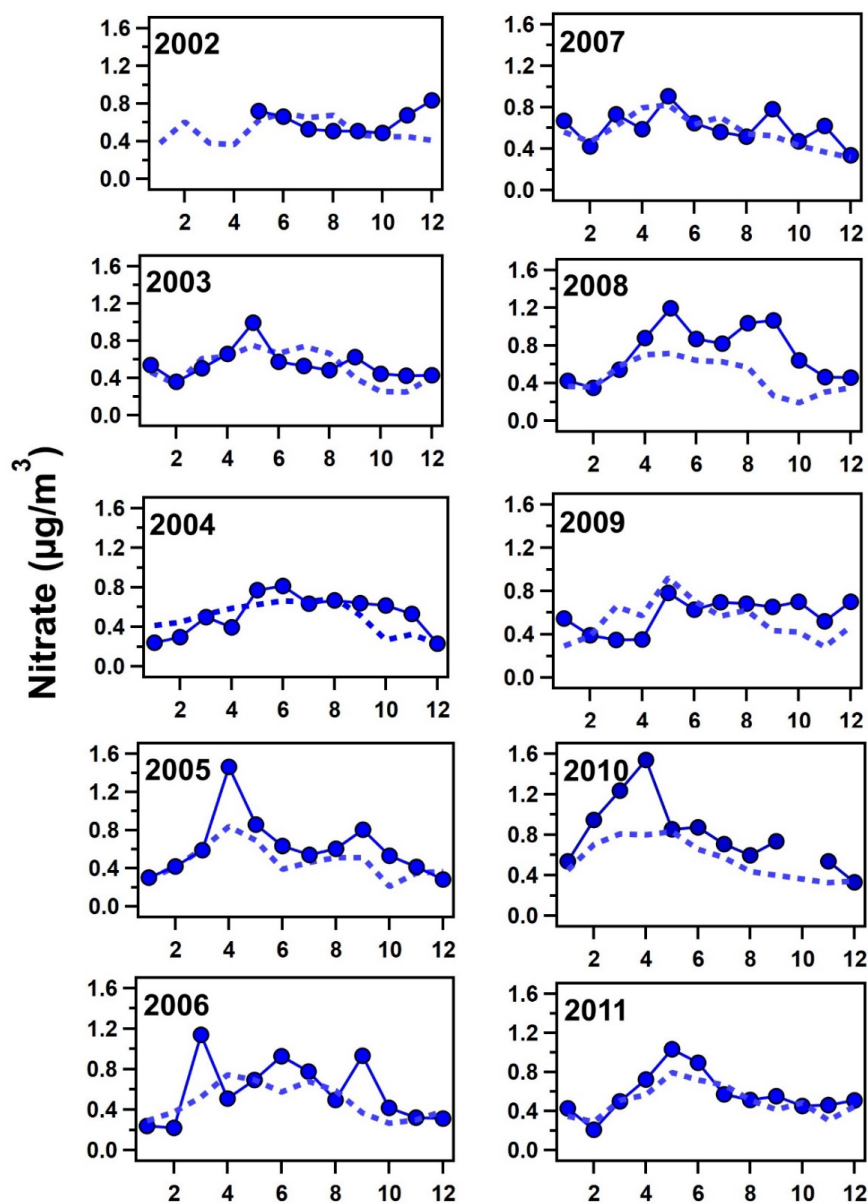
373

374 3.2 Comparison of Measured and Modeled Trends of Nitrate and Sulfate Aerosol

375 Monthly concentrations of simulated nss-sulfate and nitrate (for both the fine and coarse
376 mode combined) were compared with mass concentrations measured on filters collected at Ragged
377 Point (see Fig 7 and 8, respectively). While EQUATES predicts that nss-sulfate is almost
378 exclusively in the fine mode, nitrate concentrations are split between the fine and coarse aerosol
379 sizes with increased fine nitrate in DJF (40%) and MAM (26%) compared to JJA and SON (18%
380 for both seasons, see Fig S7) likely due to increased contributions of nitrate from fine biomass
381 burning aerosol from northern Africa in winter and spring.



382
383 **Figure 7:** Monthly averages of non-sea salt sulfate (NSS-sulfate) mass concentrations measured at
384 Barbados on filters (solid red line with red circles) compared to monthly averages of NSS-sulfate calculated
385 from EQUATES model simulations of combined fine and coarse mode sodium (Na) and sulfate using
386 equation 2 (dashed red line) for 2002-2011.



387

388 **Figure 8:** Monthly averages of nitrate mass concentrations measured in Barbados on filters (solid blue line
389 with blue circles) compared to monthly averages of combined fine and coarse mode nitrate calculated from
390 EQUATES model simulations (dashed blue line) for 2002-2011.

391

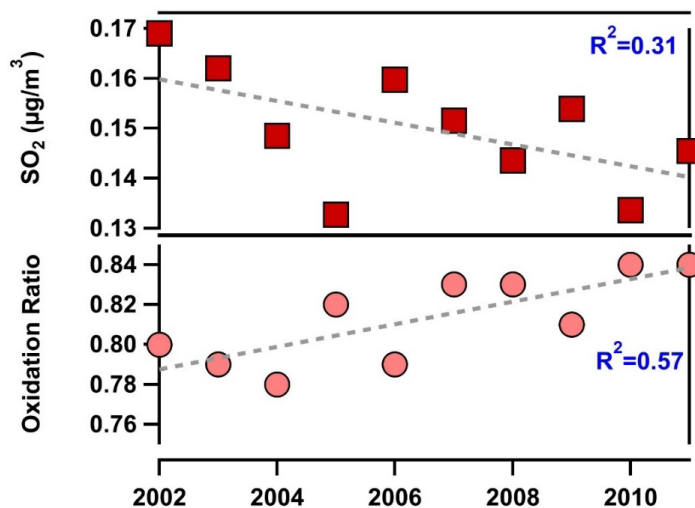
392



393 To assess the performance of the model compared to our observations, we calculated the
394 normalized mean bias (NMB) and Pearson correlation coefficient (r) for nss-sulfate and nitrate
395 (see Table S1 (Boylan & Russell, 2006)). Additional calculations of the mean bias (MB) and root-
396 mean-square error (RMSE) can also be found in Table S1 of the SI. NMB for nitrate was generally
397 within $\pm 20\%$, better than predictions of nitrate within the U.S. (Kelly et al., 2019), with the
398 exception of 2008 (-35.06%) and 2010 (-28.72%) when the model underpredicted measurements
399 likely due to the elevated African smoke transport events. The model overpredicts nss-sulfate in
400 the earlier years (2002-2007) then converges closer to our measurements at Ragged Point after
401 2008 as shown in Fig 7. The NMB for nss-sulfate also reflects this trend as high values are
402 observed in 2002 (+81.45%) then the model begins to fall within $\pm 20\%$ starting in 2008 (see Table
403 S1). As such, trends in nss-sulfate simulated by EQUATES show a decrease over time rather than
404 an increase post-2000 (see Fig S8). The decrease in EQUATES simulations of nss-sulfate post-
405 2000 compared to the increase observed in Barbados could be related to a changing bias over time.
406 For example, recent predictions for 2019 indicate CMAQ underpredicts sulfate by about 50% in
407 the eastern U.S. (45% underestimate across entire U.S.) (Vannucci et al., 2024) while previous
408 simulations for 2002 and 2016 indicated more modest normalized mean biases of 20% or less
409 (Appel et al., 2021; Sarwar et al., 2011). As a result, EQUATES may simulate a stronger decline
410 in transported U.S. sulfate over 2002-2019 than observations indicate, potentially masking
411 increasing signatures from other regions. Pearson correlation coefficients range from -0.22 to 0.88
412 by year for nitrate with a mean of 0.54. The poorest correlation (-0.22) occurs for 2002 when filter
413 observations were limited. For nss-sulfate, r ranges from 0.23 to 0.82 by year with a mean of 0.59.
414 The greatest variation between the model and measurements is for 2009 (see Fig 7), which was
415 also the year that had an erroneously high concentration of sea spray aerosol in winter. Overall,
416 the model is capturing both the magnitude and seasonal and interannual variation of nss-sulfate
417 and nitrate at our remote location in the tropical North Atlantic Basin.

418 3.2.1 Using EQUATES to Understand the Recovery in Aerosol Sulfate

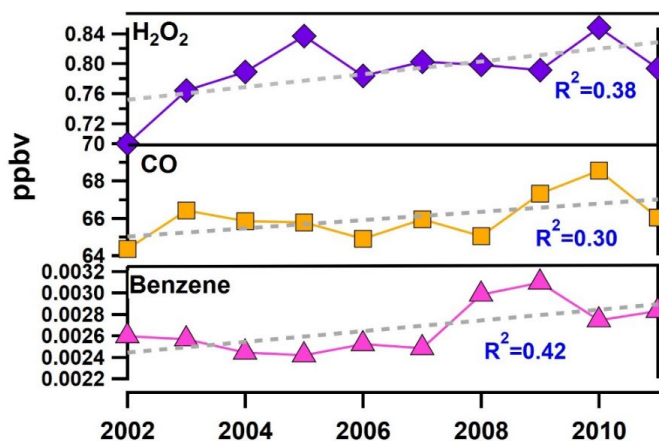
419 Figure 9 shows a decrease in $\text{SO}_2(\text{g})$ in the region near Barbados and an increase in the
420 oxidation ratio of $\text{SO}_2(\text{g})$, consistent with a predicted decrease in $\text{SO}_2(\text{g})$ and the observed increase
421 in nss-sulfate. Hydrogen peroxide (H_2O_2) concentrations also increased over this period (see Fig
422 10) and is likely linked to decreases in $\text{SO}_2(\text{g})$, which is a major sink of H_2O_2 during the aqueous
423 phase formation of sulfate (Manktelow et al., 2007). We note that the predicted oxidation ratios
424 calculated are likely an overestimate because EQUATES overpredicts nss-sulfate compared to
425 observations and the overprediction reduces with time.



426

427 **Figure 9:** Annual trends in sulfur dioxide (SO₂) simulated by the EQUATES model and the calculated
428 oxidation ratio for Ragged Point. Linear fits and corresponding correlation coefficients are also shown.

429



430

431 **Figure 10:** Annual trends in select gas phase species including benzene (pink trace, bottom panel), carbon
432 monoxide (CO) (orange trace, middle panel), and hydrogen peroxide (H₂O₂) (purple trace, top panel)
433 simulated by the EQUATES model at Ragged Point. Linear fits and corresponding correlation coefficients
434 are also shown.

435

436 Changes in biomass burning, anthropogenic emissions, oxidant concentrations, and
437 meteorological parameters were also investigated using EQUATES. Fine mode non-sea salt
438 potassium (nss-K⁺) was used as our tracer for smoke emissions. We used EQUATES data rather
439 than our nss-K⁺ observations, which were non-existent for most years from 2002-2011. No



440 significant increase in nss- K^+ was observed from our analysis (Fig S9). Meteorological parameters
441 (temperature, RH, wind speed, wind direction) were constant over time showing no shift in rainfall,
442 winds, temperature, or RH (Fig S9). Concentrations of the hydroxyl radical ($^{\bullet}OH$) did not show a
443 significant change from 2002-2011 (Fig S9). EQUATES concentrations of benzene, a tracer for
444 fossil fuel combustion, and carbon monoxide (CO), a tracer for combustion from both fossil fuels
445 and biomass burning, both increase from 2002-2011 (Fig 10). Our results suggest that
446 anthropogenic emissions in addition to an increase in the oxidation efficiency of $SO_2(g)$ to sulfate
447 are responsible for the increase of nss-sulfate post-2000.

448 4. DISCUSSION & CONCLUSIONS

449 Our over 20-year record (1990-2011) of nitrate and nss-sulfate aerosol shows two distinct
450 trends over the tropical N Atlantic Basin. Nitrate shows no significant change other than two spikes
451 in JJA and September of 2008 and MAM of 2010. Dust transport, particularly in DJF and MAM,
452 explained interannual oscillations in nitrate concentrations while increased transport of northern
453 African smoke in MAM 2010 and smoke from southern African and South America in September
454 2008 caused the increased levels of nitrate observed in those years. Nitrate has been shown to be
455 enhanced in smoke by up to 5 fold over background due to high emissions of NO_x that are rapidly
456 converted to nitrate (Adon et al., 2010; Hickman et al., 2021; Perron et al., 2022; Schlosser et al.,
457 2017). Notably, nitrate was not enhanced in JJA of 2010 even though high quantities of dust were
458 transported to Barbados. We speculate that the lack of enhanced nitrate during summer of 2010 is
459 because smoke is not co-transported with the dust during the summer season. This finding in
460 addition to our observations of enhanced nitrate associated with dust in DJF and MAM suggests
461 that the nitrate associated with African aerosol transport primarily originates from NO_x emissions
462 from African wildfires that are rapidly converted to nitrate prior to transport.

463 In contrast to the relatively flat trend in aerosol nitrate, nss-sulfate decreases by 30% from
464 1990-2000 then increases from 2000-2011, recovering to concentrations measured in the early
465 1990s. Reductions in nss-sulfate observed in Barbados are most likely due to decreased emissions
466 of SO_2 in the US and EU due to clean air policies implemented via technologies such as flue-gas
467 desulfurization devices installed in power plants (Aas et al., 2019; Kharol et al., 2017; Smith et al.,
468 2011). Thus, our results highlight that regulations aimed to improve national and regional air
469 quality also impact more distant locations such as the remote North Atlantic marine boundary layer
470 and Caribbean.

471 As shown in Fig 6, increases in SO_2 in Africa, namely from anthropogenic sources, are the
472 most probable cause for the increase in nss-sulfate levels from 2000-2011 in Barbados.
473 Anthropogenic sources of SO_2 in Africa include emissions from electricity generation, diesel
474 combustion and transportation (Assamoi & Lioussé, 2010; Keita et al., 2021; Lioussé et al., 2014),
475 refineries, gas flaring, and smelting (Doumbia et al., 2019; Osuji & Avwiri, 2005). Levels of
476 pollution in African cities are on par with Asian megacities with the largest rate of increases in
477 SO_2 observed in western Africa (Adon et al., 2016; Hopkins et al., 2009; Lioussé et al., 2014; Val
478 et al., 2013). The industrial sector in the Highveld region of South Africa also shows some of the
479 highest increases in SO_2 due to an increase in the number of coal-fired power plants arising from
480 an increased demand for electricity (Keita et al., 2021; Lioussé et al., 2014; Shikwambana et al.,



481 2020). The emissions inventory for Africa is also likely underestimated due to a lack of
482 measurements (McDuffie et al., 2020). Therefore, we speculate that anthropogenic SO₂ emissions
483 are likely higher than shown from the CEDS model and are driving the observed increases in nss-
484 sulfate in Barbados.

485 In addition to sources of SO₂ within Africa, SO₂ emissions from other nearby countries and
486 regions have been shown to be exported to Africa (Koch et al., 2007). In particular, SO₂ emissions
487 in India have rapidly risen and overtaken China as the largest emitter of SO₂ (Li et al., 2017) while
488 remote sensing observations have highlighted that SO₂ emitted from oil and gas operations in the
489 Persian Gulf have been greatly underestimated in emissions inventories (McLinden et al., 2016).
490 It is possible that these two regions may also contribute to the increase in nss-sulfate observed at
491 our measurement site.

492 While some of the increases in nss-sulfate after 2000 that occur in all seasons could be due,
493 in part, to marine biogenic, shipping, biomass burning, and volcanic emissions, their contributions
494 are likely not the dominant cause of the observed trends. Marine biogenic sulfate is estimated to
495 contribute up to 50% of nss-sulfate at Ragged Point during non-dust transport conditions (Li-Jones
496 & Prospero, 1998; Royer et al., 2023; Savoie, et al., 2002). However, our predictions of nss-sulfate
497 concentrations with EQUATES includes DMS chemistry that is not explaining our observed
498 trends. Further, a recent modeling study factoring in changes in phytoplankton dynamics found
499 that DMS emissions have not appreciably changed from the preindustrial to the present-day (Wang
500 et al., 2018). Shipping emissions likely do not explain our trends in nss-sulfate because Barbados
501 is somewhat isolated from proximal shipping impacts—heavy shipping is concentrated in the
502 Caribbean west of Barbados and along the north coast of South America (Czernański et al., 2021).
503 Biomass burning has declined in northern Africa starting in the early 2000s (Andela et al., 2017;
504 Niels Andela & Van Der Werf, 2014; Zubkova et al., 2019). Further, increased nss-sulfate has
505 been observed year-round rather than just during the main burn seasons, suggesting that this source
506 alone is likely not responsible for the major increases in nss-sulfate observed at our site. The largest
507 natural source of SO₂ in Africa is volcanic emissions from Mount Nyiragongo in the Goma region
508 of the Democratic Republic of Congo, which has been shown to impact sulfate aerosol at the
509 Amazon Tall Tower Observatory (ATTO) in Brazil (Opio et al., 2021; Saturno et al., 2018).
510 Volcanic emissions likely do impact nss-sulfate measured in Barbados but there is no evidence
511 that emissions from this source are increasing. These lines of evidence further support an
512 anthropogenic source of SO₂ as the cause of the increase in nss-sulfate observed in Barbados.

513 In addition to increased SO₂ emissions from North Africa, the oxidation ratio also increased
514 from 2002-2011, which would more efficiently convert transported SO₂ emissions from Africa to
515 sulfate. Further, concentrations of H₂O₂ increased in the post-2000 period indicating a potential
516 increase in the efficiency of aqueous phase oxidation. We would expect that even if the total burden
517 of SO₂ has been reduced globally (McDuffie et al., 2020; Smith et al., 2011), SO₂ emitted from
518 North Africa is more efficiently converted to sulfate due to greater availability of oxidants at lower
519 latitudes (Manktelow et al., 2007) and therefore have a greater impact on aerosol burdens over the
520 Caribbean than SO₂ emitted from the US and EU. It is important to note, however, that the
521 oxidation ratio calculated is most appropriate for accounting for changing oxidation efficiencies



522 of SO₂ and sulfate formation near the site, and the oxidation ratio does not account for changes in
523 the oxidation efficiency of already formed sulfate aerosol that has been transported to the site. For
524 example, SO₂ emitted from Africa might be oxidized to form sulfate prior to being transported to
525 our site.

526 One question that persists is why nitrate did not increase from 2000-2011 alongside the
527 increase in nss-sulfate? One possible explanation is a combination of reduced NO_x from smoke
528 concurrent with increased dust and smoke transport that offset any changes in nitrate other than
529 the observed spikes in 2008 and 2010. In the 2000s, biomass burning emissions declined in
530 northern equatorial Africa due to a combination of increased precipitation in DJF associated with
531 a shift from more frequent El Niño events in the 1990s to more frequent La Niña events in the
532 2000s and land use practices converting tropical savanna to cropland (Andela et al., 2017; Andela
533 & Van Der Werf, 2014; Hickman et al., 2021; Zubkova et al., 2019). The recently updated
534 Barbados dust record highlights that dust is being transported to the Caribbean earlier in the year
535 and arriving more frequently in spring (Zuidema et al., 2019), which would increase the transport
536 of biomass burning emissions and associated nitrate to the Caribbean and remote North Atlantic,
537 which may effectively cancel out the impact of reduced smoke emissions.

538 The Ragged Point site in Barbados has historically been associated with research on
539 African dust transport (Prospero et al., 2021). However, this work highlights that the site is also
540 an excellent indicator of long-term and large-scale changes in emissions and the impact of air
541 quality policies or the lack of them or poor compliance to them. Looking forward, building upon
542 the existing time series of nitrate and sulfate aerosol while also expanding the measurement
543 capabilities at Ragged Point to incorporate measurements of metals, which will increase our ability
544 to apportion aerosol sources, and carbonaceous aerosol will provide needed insight into the impact
545 of anthropogenic and biomass burning on sulfate and nitrate burdens over the remote N. Atlantic
546 that complement recent work performed in the S Atlantic (Zuidema et al., 2016, 2018).

547

548 **Data Availability Statement:** Measured nitrate, nss-sulfate, and sea salt concentrations will be
549 put on the University of Miami's repository in addition to EQUATES simulations of nitrate, nss-
550 sulfate, sea salt, gaseous tracers (SO₂, benzene, CO, H₂O₂) and meteorological parameters. Dust
551 mass concentrations from Barbados can be found in the data repository for Zuidema et al., 2019.
552 EQUATES data is available via the Remote Sensing Information Gateway (RSIG):
553 <https://www.epa.gov/hesc/remote-sensing-information-gateway>.

554

555 **Author Contribution:** CJG analyzed measurement and model data and wrote the manuscript.
556 JMP, LC, EB, PS collected data, operated the site, and analyzed filters for dust, sea salt, sulfate
557 and nitrate mass concentrations. KF and HOTP provided EQUATES model simulations and helped
558 with their interpretation. JAC performed HYSPLIT analysis. All authors read and edited the
559 manuscript.

560



561 **Competing Interests:** The authors declare that they have no conflict of interest.

562

563 **Disclaimer:** The views expressed in this paper are those of the authors and do not necessarily
564 represent the views or policies of the US Environmental Protection Agency.

565

566 **Acknowledgements:** C.J.G. acknowledges funding from an NSF CAREER grant (1944958) and
567 an NSF MRI grant (2214875). The authors acknowledge the NOAA Air Resources Laboratory
568 (ARL) for the provision of the HYSPLIT transport and dispersion model and READY website
569 (<https://www.ready.noaa.gov/HYSPLIT.php>). The authors acknowledge the family of H.C.
570 Manning and the Herbert C. Manning Trust for providing access to their land at Ragged Point. The
571 authors acknowledge the contributions of Dennis L. Savoie for his efforts to measure soluble ions
572 and dust mass concentrations from the AEROCE network. We thank Wyatt Appel, Kathleen Fahey,
573 and Jeff Willison for helpful comments that improved the quality of this manuscript.

574



575 **REFERENCES CITED**

- 576 Aas, W., Mortier, A., Bowersox, V., Cherian, R., Faluvegi, G., Fagerli, H., Hand, J., Klimont, Z.,
577 Galy-Lacaux, C., Lehmann, C. M. B., Myhre, C. L., Myhre, G., Olivie, D., Sato, K., Quaas,
578 J., Rao, P. S. P., Schulz, M., Shindell, D., Skeie, R. B., Stein, A., Takemura, T., Tsyro, S.,
579 Vet, R., & Xu, X. (2019). Global and regional trends of atmospheric sulfur. *Scientific*
580 *Reports 2019 9:1*, 9(1), 1–11. <https://doi.org/10.1038/s41598-018-37304-0>
- 581 Adams, A. M., Prospero, J. M., & Zhang, C. D. (2012). CALIPSO-derived three-dimensional
582 structure of aerosol over the Atlantic Basin and adjacent continents. *Journal of Climate*,
583 25(19), 6862–6879.
- 584 Adams, P. J., Seinfeld, J. H., & Koch, D. M. (1999). Global concentrations of tropospheric
585 sulfate, nitrate, and ammonium aerosol simulated in a general circulation model. *Journal of*
586 *Geophysical Research: Atmospheres*, 104(D11), 13791–13823.
587 <https://doi.org/10.1029/1999JD900083>
- 588 Adebisi, A. A., & Zuidema, P. (2016). The role of the southern African easterly jet in modifying
589 the southeast Atlantic aerosol and cloud environments. *Quarterly Journal of the Royal*
590 *Meteorological Society*, 142(697), 1574–1589.
- 591 Adon, M., Galy-Lacaux, C., Yoboué, V., Delon, C., Lacaux, J. P., Castera, P., Gardrat, E.,
592 Pienaar, J., Al Ourabi, H., Laouali, D., Diop, B., Sigha-Nkamdjou, L., Akpo, A., Tathy, J.
593 P., Lavenu, F., & Mougou, E. (2010). Long term measurements of sulfur dioxide, nitrogen
594 dioxide, ammonia, nitric acid and ozone in Africa using passive samplers. *Atmospheric*
595 *Chemistry and Physics*, 10(15), 7467–7487. <https://doi.org/10.5194/ACP-10-7467-2010>
- 596 Adon, Marcellin, Eronique Yobou E A, V., Galy-Lacaux, C., Lioussé, C., Diop, B., Hadji, E.,
597 Doumbia, T., Gardrat, E., Ndiaye, S. A., & Jarnot, C. (2016). Measurements of NO₂, SO₂,
598 NH₃, HNO₃ and O₃ in West African urban environments.
599 <https://doi.org/10.1016/j.atmosenv.2016.03.050>
- 600 Andela, N., Morton, D. C., Giglio, L., Chen, Y., Van Der Werf, G. R., Kasibhatla, P. S., DeFries,
601 R. S., Collatz, G. J., Hantson, S., Kloster, S., Bachelet, D., Forrest, M., Lasslop, G., Li, F.,
602 Mangeon, S., Melton, J. R., Yue, C., & Randerson, J. T. (2017). A human-driven decline in
603 global burned area. *Science*, 356(6345), 1356–1362. <https://doi.org/10.1126/science.aal4108>
- 604 Andela, Niels, & Van Der Werf, G. R. (2014). Recent trends in African fires driven by cropland
605 expansion and El Niño to La Niña transition. <https://doi.org/10.1038/NCLIMATE2313>
- 606 Andreae, M. O. (1983). Soot Carbon and Excess Fine Potassium: Long-Range Transport of
607 Combustion-Derived Aerosols. *Science*, 220(4602), 1148–1151.
608 <https://doi.org/10.1126/SCIENCE.220.4602.1148>
- 609 Andreae, M. O. (2019). Emission of trace gases and aerosols from biomass burning - An updated
610 assessment. *Atmospheric Chemistry and Physics*, 19(13), 8523–8546.
611 <https://doi.org/10.5194/ACP-19-8523-2019>
- 612 Andreae, M. O., & Merlet, P. (2001). Emission of trace gases and aerosols from biomass
613 burning. *Global Biogeochemical Cycles*, 15(4), 955–966.



- 614 Appel, B. R., Kothny, E. L., Hoffer, E. M., Hidy, G. M., & Wesolowski, J. J. (1978). Sulfate and
615 Nitrate Data from California Aerosol Characterization Experiment (Achex). *Environmental*
616 *Science & Technology*, 12(4), 418–425.
- 617 Appel, K. W., Bash, J. O., Fahey, K. M., Foley, K. M., Gilliam, R. C., Hogrefe, C., Hutzell, W.
618 T., Kang, D., Mathur, R., Murphy, B. N., Napelenok, S. L., Nolte, C. G., Pleim, J. E.,
619 Pouliot, G. A., Pye, H. O. T., Ran, L., Roselle, S. J., Sarwar, G., Schwede, D. B., Sidi, F. I.,
620 Spero, T. L., & Wong, D. C. (2021). The Community Multiscale Air Quality (CMAQ)
621 model versions 5.3 and 5.3.1: system updates and evaluation. *Geosci. Model Dev*, 14, 2867–
622 2897. <https://doi.org/10.5194/gmd-14-2867-2021>
- 623 Assamoi, E. M., & Liousse, C. (2010). A new inventory for two-wheel vehicle emissions in West
624 Africa for 2002. *Atmospheric Environment*, 44(32), 3985–3996.
625 <https://doi.org/10.1016/J.ATMOSENV.2010.06.048>
- 626 Barkley, A. E., Prospero, J. M., Mahowald, N., Hamilton, D. S., Popendorf, K. J., Oehlert, A.
627 M., Pourmand, A., Gatineau, A., Panechou-Pulcherie, K., Blackwelder, P., & Gaston, C. J.
628 (2019). African biomass burning is a substantial source of phosphorus deposition to the
629 Amazon, Tropical Atlantic Ocean, and Southern Ocean. *Proceedings of the National*
630 *Academy of Sciences of the United States of America*, 116(33), 16216–16221.
631 <https://doi.org/10.1073/pnas.1906091116>
- 632 Benish, S. E., Bash, J. O., Foley, K. M., Appel, K. W., Hogrefe, C., Gilliam, R., & Pouliot, G.
633 (2022). Long-term regional trends of nitrogen and sulfur deposition in the United States
634 from 2002 to 2017. *Atmospheric Chemistry and Physics*, 22(19), 12749–12767.
635 <https://doi.org/10.5194/ACP-22-12749-2022>
- 636 Boylan, J. W., & Russell, A. G. (2006). PM and light extinction model performance metrics,
637 goals, and criteria for three-dimensional air quality models. *Atmospheric Environment*, 40,
638 4946–4959. <https://doi.org/10.1016/j.atmosenv.2005.09.087>
- 639 Carlson, T. N., & Prospero, J. M. (1972). The large-scale movement of Saharan air outbreaks
640 over the Northern Equatorial Atlantic. *Journal of Applied Meteorology*, aa(2), 283–297.
- 641 Carslaw, K. S. ., Lee, L. A. ., Reddington, C. L. ., Pringle, K. J. ., Rap, A. ., Forster, P. M. .,
642 Mann, G. W. ., Spracklen, D. V. ., Woodhouse, M. T. ., Regayre, L. A. ., & Pierce, J. R.
643 (2013). Large contribution of natural aerosols to uncertainty in indirect forcing. *Nature*,
644 503, doi:10.1038/nature12674.
- 645 Charlson, R. J., Schwartz, S. E., Hales, J. M., Cess, R. D., Coakley, J. A., Hansen, J. E., &
646 Hofmann, D. J. (1992). Climate Forcing by Anthropogenic Aerosols. *Science*, 255(5043),
647 423–430. <https://doi.org/10.1126/SCIENCE.255.5043.423>
- 648 Chiapello, I., Moulin, C., & Prospero, J. M. (2005). Understanding the long-term variability of
649 African dust transport across the Atlantic as recorded in both Barbados surface
650 concentrations and large-scale Total Ozone Mapping Spectrometer (TOMS) optical
651 thickness. *Journal of Geophysical Research: Atmospheres*, 110(D18), 1–9.
652 <https://doi.org/10.1029/2004JD005132>
- 653 Czermański, E., Cirella, G. T., Notteboom, T., Oniszczyk-Jastrzabek, A., & Pawłowska, B.
654 (2021). An Energy Consumption Approach to Estimate Air Emission Reductions in



- 655 Container Shipping. *Energies* 2021, Vol. 14, Page 278, 14(2), 278.
656 <https://doi.org/10.3390/EN14020278>
- 657 Doherty, O. M., Riemer, N., & Hameed, S. (2008). Saharan mineral dust transport into the
658 Caribbean: Observed atmospheric controls and trends. *Journal of Geophysical Research:*
659 *Atmospheres*, 113(D7). <https://doi.org/10.1029/2007JD009171>
- 660 Doherty, O. M., Riemer, N., & Hameed, S. (2012). Control of Saharan mineral dust transport to
661 Barbados in winter by the Intertropical Convergence Zone over West Africa. *Journal of*
662 *Geophysical Research: Atmospheres*, 117(D19), 19117.
663 <https://doi.org/10.1029/2012JD017767>
- 664 Doumbia, E. H. T., Liousse, C., Keita, S., Granier, L., Granier, C., Elvidge, C. D., Elguindi, N.,
665 & Law, K. (2019). Flaring emissions in Africa: Distribution, evolution and comparison with
666 current inventories. *Atmospheric Environment*, 199, 423–434.
667 <https://doi.org/10.1016/J.ATMOSENV.2018.11.006>
- 668 Draxler, R. R., & Rolph, G. D. (2011). HYSPLIT (HYbrid Single-Particle Lagrangian Integrated
669 Trajectory) Model access via NOAA ARL READY Website
670 (<http://ready.arl.noaa.gov/HYSPLIT.php>). *NOAA Air Resources Laboratory*, Silver Spring,
671 MD.
- 672 Foley, K. M., Pouliot, G. A., Eyth, A., Aldridge, M. F., Allen, C., Appel, K. W., Bash, J. O.,
673 Beardsley, M., Beidler, J., Choi, D., Farkas, C., Gilliam, R. C., Godfrey, J., Henderson, B.
674 H., Hogrefe, C., Koplitz, S. N., Mason, R., Mathur, R., Misenis, C., Possiel, N., Pye, H. O.
675 T., Reynolds, L., Roark, M., Roberts, S., Schwede, D. B., Seltzer, K. M., Sonntag, D.,
676 Talgo, K., Toro, C., Vukovich, J., Xing, J., & Adams, E. (2023). 2002–2017 anthropogenic
677 emissions data for air quality modeling over the United States. *Data in Brief*, 47, 109022.
678 <https://doi.org/10.1016/J.DIB.2023.109022>
- 679 Galloway, J. N., Townsend, A. R., Erisman, J. W., Bekunda, M., Cai, Z., Freney, J. R.,
680 Martinelli, L. A., Seitzinger, S. P., & Sutton, M. A. (2008). Transformation of the nitrogen
681 cycle: Recent trends, questions, and potential solutions. *Science*, 320(5878), 889–892.
682 <https://doi.org/10.1126/SCIENCE.1136674>
- 683 Giglio, L., Randerson, J. T., & van der Werf, G. R. (2013). Analysis of daily, monthly, and
684 annual burned area using the fourth-generation global fire emissions database (GFED4).
685 *Journal of Geophysical Research-Biogeosciences*, 118(1), 317–328.
- 686 Giglio, Louis, Csizsar, I., & Justice, C. O. (2006). Global distribution and seasonality of active
687 fires as observed with the Terra and Aqua Moderate Resolution Imaging Spectroradiometer
688 (MODIS) sensors. *Journal of Geophysical Research: Biogeosciences*, 111(2).
689 <https://doi.org/10.1029/2005JG000142>
- 690 Goudie, A. S., & Middleton, N. J. (2001). Saharan dust storms: nature and consequences. *Earth-*
691 *Science Reviews*, 56(1–4), 179–204. [https://doi.org/10.1016/S0012-8252\(01\)00067-8](https://doi.org/10.1016/S0012-8252(01)00067-8)
- 692 Hand, J. L., Schichtel, B. A., Malm, W. C., & Pitchford, M. L. (2012). Particulate sulfate ion
693 concentration and SO₂ emission trends in the United States from the early 1990s through
694 2010. *Atmospheric Chemistry and Physics*, 12(21), 10353–10365.



- 695 Hickman, J. E., Andela, N., Tsigaridis, K., Galy-Lacaux, C., Ossohou, M., & Bauer, S. E.
696 (2021). Reductions in NO₂ burden over north equatorial Africa from decline in biomass
697 burning in spite of growing fossil fuel use, 2005 to 2017. *Proceedings of the National*
698 *Academy of Sciences of the United States of America*, 118(7).
699 <https://doi.org/10.1073/PNAS.2002579118/-/DCSUPPLEMENTAL>
- 700 Hopkins, J. R., Evans, M. J., Lee, J. D., Lewis, A. C., Marsham, J. H., McQuaid, J. B., Parker, D.
701 J., Stewart, D. J., Reeves, C. E., & Purvis, R. M. (2009). Direct estimates of emissions from
702 the megacity of Lagos. *Atmospheric Chemistry and Physics*, 9(21), 8471–8477.
703 <https://doi.org/10.5194/ACP-9-8471-2009>
- 704 <https://gispub.epa.gov/air/trendsreport/2023/>. (2023). Retrieved from
705 <https://gispub.epa.gov/air/trendsreport/2023/>
- 706 Jickells, T. D., Buitenhuis, E., Altieri, K., Baker, A. R., Capone, D., Duce, R. A., Dentener, F.,
707 Fennel, K., Kanakidou, M., LaRoche, J., Lee, K., Liss, P., Middelburg, J. J., Moore, J. K.,
708 Okin, G., Oschlies, A., Sarin, M., Seitzinger, S., Sharples, J., Singh, A., Suntharalingam, P.,
709 Uematsu, M., & Zamora, L. M. (2017). A reevaluation of the magnitude and impacts of
710 anthropogenic atmospheric nitrogen inputs on the ocean. *Global Biogeochemical Cycles*,
711 31(2), 289–305. <https://doi.org/10.1002/2016GB005586>
- 712 Keene, W. C., Pszenny, A. A. P., Galloway, J. N., & Hawley, M. E. (1986). Sea-salt corrections
713 and interpretation of constituent ratios in marine precipitation. *Journal of Geophysical*
714 *Research*, 91(D6), 6647. <https://doi.org/10.1029/JD091ID06P06647>
- 715 Keene, W. C., Moody, J. L., Galloway, J. N., Prospero, J. M., Cooper, O. R., Eckhardt, S., &
716 Maben, J. R. (2014). Long-term trends in aerosol and precipitation composition over the
717 western North Atlantic Ocean at Bermuda. *Atmospheric Chemistry and Physics*, 14(15),
718 8119–8135.
- 719 Keita, S., Lioussé, C., Assamoi, E. M., Doumbia, T., N’Datchoh, E. T., Gnamien, S., Elguindi,
720 N., Granier, C., & Yoboué, V. (2021). African anthropogenic emissions inventory for gases
721 and particles from 1990 to 2015. *Earth System Science Data*, 13(7), 3691–3705.
722 <https://doi.org/10.5194/ESSD-13-3691-2021>
- 723 Kelly, J. T., Koplitz, S. N., Baker, K. R., Holder, A. L., Pye, H. O. T., Murphy, B. N., Bash, J.
724 O., Henderson, B. H., Possiel, N. C., Simon, H., Eyth, A. M., Jang, C., Phillips, S., &
725 Timin, B. (2019). Assessing PM 2.5 model performance for the conterminous U.S. with
726 comparison to model performance statistics from 2007–2015. *Atmos Environ*, 214,
727 <https://doi.org/10.1016/j.atmosenv.2019.116872>.
728 <https://doi.org/10.1016/j.atmosenv.2019.116872>
- 729 Kharol, S. K., McLinden, C. A., Sioris, C. E., Shephard, M. W., Fioletov, V., Van Donkelaar, A.,
730 Philip, S., & Martin, R. V. (2017). OMI satellite observations of decadal changes in ground-
731 level sulfur dioxide over North America. *Atmos. Chem. Phys*, 17, 5921–5929.
732 <https://doi.org/10.5194/acp-17-5921-2017>
- 733 Koch, D., Bond, T. C., Streets, D., Unger, N., & van der Werf, G. R. (2007). Global impacts of
734 aerosols from particular source regions and sectors. *Journal of Geophysical Research:*
735 *Atmospheres*, 112(D2), 2205. <https://doi.org/10.1029/2005JD007024>



- 736 Kramer, S. J., Kirtman, B. P., Zuidema, P., & Ngan, F. (2020). Subseasonal Variability of
737 Elevated Dust Concentrations Over South Florida. *Journal of Geophysical Research:*
738 *Atmospheres*, 125(6). <https://doi.org/10.1029/2019JD031874>
- 739 Lelieveld, J., & Heintzenberg, J. (1992). Sulfate cooling effect on climate through in-cloud
740 processing of anthropogenic SO₂. *Science*, 258, 117–120.
- 741 Lelieveld, J., Berresheim, H., Borrmann, S., Crutzen, P. J., Dentener, F. J., Fischer, H., Feichter,
742 J., Flatau, P. J., Heland, J., Holzinger, R., Korrmann, R., Lawrence, M. G., Levin, Z.,
743 Markowicz, K. M., Mihalopoulos, N., Minikin, A., Ramanathan, V., De Reus, M., Roelofs,
744 G. J., Scheeren, H. A., Sciare, J., Schlager, H., Schultz, M., Siegmund, P., Steil, B.,
745 Stephanou, E. G., Stier, P., Traub, M., Warneke, C., Williams, J., & Ziereis, H. (2002).
746 Global air pollution crossroads over the Mediterranean. *Science*, 298(5594), 794–799.
747 [https://doi.org/10.1126/SCIENCE.1075457/ASSET/9D6C7086-E45D-4A4D-9892-](https://doi.org/10.1126/SCIENCE.1075457/ASSET/9D6C7086-E45D-4A4D-9892-2054F591C047/ASSETS/GRAPHIC/SE4120969007.JPEG)
748 [2054F591C047/ASSETS/GRAPHIC/SE4120969007.JPEG](https://doi.org/10.1126/SCIENCE.1075457/ASSET/9D6C7086-E45D-4A4D-9892-2054F591C047/ASSETS/GRAPHIC/SE4120969007.JPEG)
- 749 Lelieveld, J., Hoor, P., Jöckel, P., Pozzer, A., Hadjinicolaou, P., Cammas, J. P., & Beirle, S.
750 (2009). Severe ozone air pollution in the Persian Gulf region. *Atmospheric Chemistry and*
751 *Physics*, 9(4), 1393–1406. <https://doi.org/10.5194/ACP-9-1393-2009>
- 752 Li-Jones, X., & Prospero, J. M. (1998). Variations in the size distribution of non-sea-salt sulfate
753 aerosol in the marine boundary layer at Barbados: Impact of African dust. *Journal of*
754 *Geophysical Research-Atmospheres*, 103(D13), 16073–16084.
- 755 Li, C., McLinden, C., Fioletov, V., Krotkov, N., Carn, S., Joiner, J., Streets, D., He, H., Ren, X.,
756 Li, Z., & Dickerson, R. R. (2017). India Is Overtaking China as the World’s Largest Emitter
757 of Anthropogenic Sulfur Dioxide. *Scientific Reports 2017 7:1*, 7(1), 1–7.
758 <https://doi.org/10.1038/s41598-017-14639-8>
- 759 Liousse, C., Assamoi, E., Criqui, P., Granier, C., & Rosset, R. (2014). Explosive growth in
760 African combustion emissions from 2005 to 2030. *Environmental Research Letters*, 9(3).
- 761 Mahowald, N. ., Scanza, R., Brahney, J., Goodale, C. L. ., Hess, P. G. ., Moore, J. K., & Neff, J.
762 (2017). Aerosol deposition impacts on land and ocean carbon cycles. *Curr Clim Change*
763 *Rep*, 3, 16–31.
- 764 Manktelow, P. T., Mann, G. W., Carslaw, K. S., Spracklen, D. V., & Chipperfield, M. P. (2007).
765 Regional and global trends in sulfate aerosol since the 1980s. *Geophysical Research Letters*,
766 34(14), 14803. <https://doi.org/10.1029/2006GL028668>
- 767 Mathur, R., Xing, J., Gilliam, R., Sarwar, G., Hogrefe, C., Pleim, J., Pouliot, G., Roselle, S.,
768 Spero, T. L., Wong, D. C., & Young, J. (2017). Extending the Community Multiscale Air
769 Quality (CMAQ) modeling system to hemispheric scales: overview of process
770 considerations and initial applications. *Atmos. Chem. Phys*, 17, 12449–12474.
771 <https://doi.org/10.5194/acp-17-12449-2017>
- 772 McDuffie, E. E., Smith, S. J., O’rourke, P., Tibrewal, K., Venkataraman, C., Marais, E. A.,
773 Zheng, B., Crippa, M., Brauer, M., & Martin, R. V. (2020). A global anthropogenic
774 emission inventory of atmospheric pollutants from sector-and fuel-specific sources (1970-
775 2017): an application of the Community Emissions Data System (CEDS). *Earth Syst. Sci.*
776 *Data*, 12, 3413–3442. <https://doi.org/10.5194/essd-12-3413-2020>



- 777 McDuffie, E. E., Smith, S. J., O'Rourke, P., Tibrewal, K., Venkataraman, C., Marais, E. A.,
778 Zheng, B., Crippa, M., Brauer, M., & Martin, R. V. (2020). A global anthropogenic
779 emission inventory of atmospheric pollutants from sector- And fuel-specific sources (1970-
780 2017): An application of the Community Emissions Data System (CEDS). *Earth System
781 Science Data*, 12(4), 3413–3442. <https://doi.org/10.5194/ESSD-12-3413-2020>
- 782 McLinden, C. A., Fioletov, V., Shephard, M. W., Krotkov, N., Li, C., Martin, R. V, Moran, M.
783 D., & Joiner, J. (2016). Space-based detection of missing sulfur dioxide sources of global
784 air pollution. <https://doi.org/10.1038/NGEO2724>
- 785 Murphy, D. M., Cziczo, D. J., Froyd, K. D., Hudson, P. K., Matthew, B. M., Middlebrook, A.
786 M., Peltier, R. E., Sullivan, A., Thomson, D. S., & Weber, R. J. (2006). Single-particle mass
787 spectrometry of tropospheric aerosol particles. *Journal of Geophysical Research-
788 Atmospheres*, 111(D23), D23S32, doi:10.1029/2006JD007340.
- 789 Opio, R., Mugume, I., & Nakatumba-Nabende, J. (2021). Understanding the Trend of NO₂, SO₂
790 and CO over East Africa from 2005 to 2020. *Atmosphere 2021, Vol. 12, Page 1283*, 12(10),
791 1283. <https://doi.org/10.3390/ATMOS12101283>
- 792 Osuji, L. C., & Awwiri, G. O. (2005). Flared Gases and Other Pollutants Associated with Air
793 Quality in Industrial Areas of Nigeria: An Overview. *Chemistry & Biodiversity*, 2(10),
794 1277–1289. <https://doi.org/10.1002/CBDV.200590099>
- 795 Perron, M. M. G., Meyerink, S., Corkill, M., Strzelec, M., Proemse, B. C., Gault-Ringold, M.,
796 Sanz Rodriguez, E., Chase, Z., & Bowie, A. R. (2022). Trace elements and nutrients in
797 wildfire plumes to the southeast of Australia. *Atmospheric Research*, 270, 106084.
798 <https://doi.org/10.1016/J.ATMOSRES.2022.106084>
- 799 Prospero, J. M. (1999). Long-term measurements of the transport of African mineral dust to the
800 southeastern United States: Implications for regional air quality. *Journal of Geophysical
801 Research-Atmospheres*, 104(D13), 15917–15927.
- 802 Prospero, J. M., & Mayol-Bracero, O. L. (2013). Understanding the transport and impact of
803 African dust on the Caribbean Basin. *Bulletin of the American Meteorological Society*,
804 94(9), 1329–1337.
- 805 Prospero, J. M., Glaccum, R. A. ., & Nees, R. T. (1981). Atmospheric transport of soil dust from
806 Africa to South America. *Nature*, 289, 570–572.
- 807 Prospero, J. M., Olmez, I., & Ames, M. (2001). Al AND Fe IN PM 2.5 AND PM 10
808 SUSPENDED PARTICLES IN SOUTH-CENTRAL FLORIDA: THE IMPACT OF THE
809 LONG RANGE TRANSPORT OF AFRICAN MINERAL DUST.
- 810 Prospero, J. M., Collard, F.-X., Molinie, J., & Jeannot, A. (2014). Characterizing the annual
811 cycle of African dust transport to the Caribbean Basin and South America and its impact on
812 the environment and air quality. *Global Biogeochemical Cycles*, 29, 757–773.
813 <https://doi.org/10.1111/1462-2920.13280>
- 814 Prospero, J. M., Delany, A. C., Delany, A. C., & Carlson, T. N. (2021). The Discovery of
815 African Dust Transport to the Western Hemisphere and the Saharan Air Layer: A History.
816 *Bulletin of the American Meteorological Society*, 102(6), E1239–E1260.



- 817 <https://doi.org/10.1175/BAMS-D-19-0309.1>
- 818 Quinn, P. K., Bates, T. S., Coffman, D. J., Upchurch, L. M., Johnson, J. E., Brewer, A., Baidar,
819 S., McCoy, I. L., & Zuidema, P. (2022). Wintertime Observations of Tropical Northwest
820 Atlantic Aerosol Properties During ATOMIC: Varying Mixtures of Dust and Biomass
821 Burning. *Journal of Geophysical Research: Atmospheres*, 127(8), e2021JD036253.
822 <https://doi.org/10.1029/2021JD036253>
- 823 Rafaj, P., Amann, M., Siri, J., & Wuester, H. (2015). Changes in European greenhouse gas and
824 air pollutant emissions 1960–2010: decomposition of determining factors. *Uncertainties in*
825 *Greenhouse Gas Inventories*, 27–54. https://doi.org/10.1007/978-3-319-15901-0_3
- 826 Rickly, P. S., Guo, H., Campuzano-Jost, P., Jimenez, J. L., Wolfe, G. M., Bennett, R., Bourgeois,
827 L., Crounse, J. D., Dibb, J. E., DiGangi, J. P., Diskin, G. S., Dollner, M., Gargulinski, E. M.,
828 Hall, S. R., Halliday, H. S., Hanisco, T. F., Hannun, R. A., Liao, J., Moore, R., Nault, B. A.,
829 Nowak, J. B., Peischl, J., Robinson, C. E., Ryerson, T., Sanchez, K. J., Schöberl, M., Soja,
830 A. J., St Clair, J. M., Thornhill, K. L., Ullmann, K., Wennberg, P. O., Weinzierl, B.,
831 Wiggins, E. B., Winstead, E. L., & Rollins, A. W. (2022). Emission factors and evolution of
832 SO₂ measured from biomass burning in wildfires and agricultural fires. *Atmos. Chem.*
833 *Phys*, 22, 15603–15620. <https://doi.org/10.5194/acp-22-15603-2022>
- 834 Roberts, G., Wooster, M. J., & Lagoudakis, E. (2009). Annual and diurnal African biomass
835 burning temporal dynamics. *Biogeosciences*, 6(5), 849–866. [https://doi.org/10.5194/BG-6-](https://doi.org/10.5194/BG-6-849-2009)
836 849-2009
- 837 Rolph, G., Stein, A., & Stunder, B. (2017). Real-time Environmental Applications and Display
838 sYstem: READY. *Environmental Modelling & Software*, 95, 210–228.
- 839 Royer, H. M., Pöhlker, M. L., Krüger, O., Blades, E., Sealy, P., Lata, N. N., Cheng, Z., China, S.,
840 Ault, A. P., Quinn, P. K., Zuidema, P., Pöhlker, C., Pöschl, U., Andreae, M., & Gaston, C.
841 J. (2023). African smoke particles act as cloud condensation nuclei in the wintertime
842 tropical North Atlantic boundary layer over Barbados. *Atmospheric Chemistry and Physics*,
843 23(2), 981–998. <https://doi.org/10.5194/ACP-23-981-2023>
- 844 Sarwar, G., Fahey, K. M., Napelenok, S. L., Roselle, S. J., & Mathur, R. (2011). Examining the
845 impact of CMAQ model updates on aerosol sulfate predictions. In *The 10th Annual CMAS*
846 *Models-3 User's Conference* (p. vol 775). Chapel Hill, NC.
- 847 Sarwar, G., Hogrefe, C., Henderson, B. H., Foley, K., Mathur, R., Murphy, B., & Ahmed, S.
848 (2023). Characterizing variations in ambient PM_{2.5} concentrations at the U.S. Embassy in
849 Dhaka, Bangladesh using observations and the CMAQ modeling system. *Atmospheric*
850 *Environment*, 296, 119587. <https://doi.org/10.1016/J.ATMOSENV.2023.119587>
- 851 Saturno, J., Ditas, F., Penning De Vries, M., Holanda, B. A., Pöhlker, M. L., Carbone, S., Walter,
852 D., Bobrowski, N., Brito, J., Chi, X., Gutmann, A., Hrabe De Angelis, I., Machado, L. A.
853 T., Moran-Zuloaga, D., Rüdiger, J., Schneider, J., Schulz, C., Wang, Q., Wendisch, M.,
854 Artaxo, P., Wagner, T., Pöschl, U., Andreae, M. O., & Pöhlker, C. (2018). African volcanic
855 emissions influencing atmospheric aerosol particles over the Amazon rain forest.
856 *Atmospheric Chemistry and Physics*, 18, 10391–10405. [https://doi.org/10.5194/acp-2017-](https://doi.org/10.5194/acp-2017-1152)
857 1152



- 858 Savoie, D.L., Arimoto, R., Keene, W. C., Prospero, J. M., Duce, R. A., & Galloway, J. N.
859 (2002). Marine biogenic and anthropogenic contributions to non-sea-salt sulfate in the
860 marine boundary layer over the North Atlantic Ocean. *Journal of Geophysical Research-*
861 *Atmospheres*, 107(D18), 4356, doi:10.1029/2001JD000970.
- 862 Savoie, D. L., & Prospero, J. M. (1982). Particle Size Distribution of Nitrate and Sulfate in the
863 Marine Atmosphere. *Geophysical Research Letters*, 9(10), 1207–1210.
- 864 Savoie, D. L. ., & Prospero, J. M. . (1980). Water-soluble potassium, calcium, and magnesium in
865 the aerosols over the tropical North Atlantic. *Journal of Geophysical Research: Oceans*,
866 85(C1), 385–392. <https://doi.org/10.1029/JC085IC01P00385>
- 867 Schlosser, J. S., Braun, R. A., Bradley, T., Dadashazar, H., MacDonald, A. B., Aldhaif, A. A.,
868 Aghdam, M. A., Mardi, A. H., Xian, P., & Sorooshian, A. (2017). Analysis of aerosol
869 composition data for western United States wildfires between 2005 and 2015: Dust
870 emissions, chloride depletion, and most enhanced aerosol constituents. *Journal of*
871 *Geophysical Research: Atmospheres*, 122(16), 8951–8966.
872 <https://doi.org/10.1002/2017JD026547>
- 873 Shah, V., Jaeglé, L., Thornton, J. A., Lopez-Hilfiker, F. D., Lee, B. H., Schroder, J. C.,
874 Campuzano-Jost, P., Jimenez, J. L., Guo, H., Sullivan, A. P., Weber, R. J., Green, J. R.,
875 Fiddler, M. N., Bililign, S., Campos, T. L., Stell, M., Weinheimer, A. J., Montzka, D. D., &
876 Brown, S. S. (2018). Chemical feedbacks weaken the wintertime response of particulate
877 sulfate and nitrate to emissions reductions over the eastern United States. *Proceedings of the*
878 *National Academy of Sciences of the United States of America*, 115(32), 8110–8115.
879 <https://doi.org/10.1073/PNAS.1803295115>
- 880 Shikwambana, L., Mhangara, P., & Mbatha, N. (2020). Trend analysis and first time
881 observations of sulphur dioxide and nitrogen dioxide in South Africa using
882 TROPOMI/Sentinel-5 P data. *International Journal of Applied Earth Observation and*
883 *Geoinformation*, 91, 102130. <https://doi.org/10.1016/J.JAG.2020.102130>
- 884 Smith, S. J., Van Aardenne, J., Klimont, Z., Andres, R. J., Volke, A., & Delgado Arias, S.
885 (2011). Anthropogenic sulfur dioxide emissions: 1850-2005. *Atmospheric Chemistry and*
886 *Physics*, 11(3), 1101–1116. <https://doi.org/10.5194/ACP-11-1101-2011>
- 887 Stein, A. F., Draxler, R. R., Rolph, G. D., Stunder, B. J. B., Cohen, M. D., & Ngan, F. (2015).
888 Noaa's Hysplit Atmospheric Transport and Dispersion Modeling System. *Bulletin of the*
889 *American Meteorological Society*, 96(12), 2059–2077.
- 890 Taylor, S. R. ., & McLennan, S. M. . (1985). *The continental crust: Its composition and*
891 *evolution*. Oxford: Blackwell Scientific Publications.
- 892 Trapp, J. M. ., Millero, F. J. ., & Prospero, J. M. (2010). Trends in the solubility of iron in dust-
893 dominated aerosols in the equatorial Atlantic trade winds: Importance of iron speciation and
894 sources. *Geochemistry, Geophysics, Geosystems*, 11(Q03014), doi:10.1029/2009GC002651.
895 Retrieved from internal-pdf://106.0.179.6/Trapp_et_al-2010-
896 Geochemistry,_Geophysics,_Geo.pdf
- 897 Tsamalis, C., Chédin, A., Pelon, J., & Capelle, V. (2013). The seasonal vertical distribution of
898 the saharan air layer and its modulation by the wind. *Atmospheric Chemistry and Physics*,



- 899 13(22), 11235–11257. <https://doi.org/10.5194/ACP-13-11235-2013>
- 900 Val, S., Lioussé, C., Doumbia, E. H. T., Galy-Lacaux, C., Cachier, H., Marchand, N., Badel, A.,
901 Gardrat, E., Sylvestre, A., & Baeza-Squiban, A. (2013). Physico-chemical characterization
902 of African urban aerosols (Bamako in Mali and Dakar in Senegal) and their toxic effects in
903 human bronchial epithelial cells: Description of a worrying situation. *Particle and Fibre
904 Toxicology*, 10(1), 1–16. <https://doi.org/10.1186/1743-8977-10-10/FIGURES/8>
- 905 Vannucci, P. F. ., Foley, K., Murphy, B. N. ., Hogrefe, C., Cohen, R. C. ., & Pye, H. O. T. .
906 (2024). Temperature-dependent composition of summertime PM_{2.5} in observations and
907 model predictions across the Eastern U.S. *ACS Earth and Space Chemistry*, Submitted.
- 908 Vasilakos, P., Russell, A., Weber, R., & Nenes, A. (2018). Understanding nitrate formation in a
909 world with less sulfate. *Atmospheric Chemistry and Physics*, 18(17), 12765–12775.
910 <https://doi.org/10.5194/ACP-18-12765-2018>
- 911 Wang, S., Maltrud, M., Elliott, S., Cameron-Smith, P., & Jonko, A. (2018). Influence of
912 dimethyl sulfide on the carbon cycle and biological production. *Biogeochemistry*, 138, 49–
913 68. <https://doi.org/10.1007/s10533-018-0430-5>
- 914 Van der Werf, G. R., Randerson, J. T., Collatz, G. J., & Giglio, L. (2003). Carbon emissions
915 from fires in tropical and subtropical ecosystems. *Global Change Biology*, 9(4), 547–562.
916 <https://doi.org/10.1046/J.1365-2486.2003.00604.X>
- 917 Wex, H., Dieckmann, K., Roberts, G. C., Conrath, T., Izaguirre, M. A., Hartmann, S., Herenz, P.,
918 Schafer, M., Ditas, F., Schmeissner, T., Henning, S., Wehner, B., Siebert, H., & Stratmann,
919 F. (2016). Aerosol arriving on the Caribbean island of Barbados: physical properties and
920 origin. *Atmospheric Chemistry and Physics*, 16(22), 14107–14130.
- 921 Wiedinmyer, C., Akagi, S. K., Yokelson, R. J., Emmons, L. K., Al-Saadi, J. A., Orlando, J. J., &
922 Soja, A. J. (2011). The Fire INventory from NCAR (FINN): a high resolution global model
923 to estimate the emissions from open burning. *Geosci. Model Dev*, 4, 625–641.
924 <https://doi.org/10.5194/gmd-4-625-2011>
- 925 Wolter, K., & Timlin, M. S. (2011). El Niño/Southern Oscillation behaviour since 1871 as
926 diagnosed in an extended multivariate ENSO index (MEI.ext). *International Journal of
927 Climatology*, 31(7), 1074–1087. <https://doi.org/10.1002/JOC.2336>
- 928 Yang, Y., Lou, S., Wang, H., Wang, P., & Liao, H. (2020). Trends and source apportionment of
929 aerosols in Europe during 1980-2018. *Atmospheric Chemistry and Physics*, 20(4), 2579–
930 2590. <https://doi.org/10.5194/ACP-20-2579-2020>
- 931 Zhang, T., Hoell, A., Perlwitz, J., Eischeid, J., Murray, D., Hoerling, M., & Hamill, T. M.
932 (2019). Towards Probabilistic Multivariate ENSO Monitoring. *Geophysical Research
933 Letters*, 46(17–18), 10532–10540. <https://doi.org/10.1029/2019GL083946>
- 934 Zhao, B., Jiang, J. H., Gu, Y., Diner, D., Worden, J., Liou, K. N., Su, H., Xing, J., Garay, M., &
935 Huang, L. (2017). Decadal-scale trends in regional aerosol particle properties and their
936 linkage to emission changes. *Environmental Research Letters*, 12(5), 054021.
937 <https://doi.org/10.1088/1748-9326/AA6CB2>
- 938 Zubkova, M., Boschetti, L., Abatzoglou, J. T., & Giglio, L. (2019). Changes in Fire Activity in



- 939 Africa from 2002 to 2016 and Their Potential Drivers. *Geophysical Research Letters*, 46,
940 7643–7653. <https://doi.org/10.1029/2019GL083469>
- 941 Zuidema, P., Redemann, J., Haywood, J., Wood, R., Piketh, S., Hipondoka, M., & Formenti, P.
942 (2016). Smoke and Clouds above the Southeast Atlantic: Upcoming Field Campaigns Probe
943 Absorbing Aerosol’s Impact on Climate. *Bulletin of the American Meteorological Society*,
944 97(7), 1131–1135. <https://doi.org/10.1175/BAMS-D-15-00082.1>
- 945 Zuidema, P., Sedlacek, A. J., Flynn, C., Springston, S., Delgadillo, R., Zhang, J., Aiken, A. C.,
946 Koontz, A., & Muradyan, P. (2018). The Ascension Island Boundary Layer in the Remote
947 Southeast Atlantic is Often Smoky. *Geophysical Research Letters*, 45(9), 4456–4465.
948 <https://doi.org/10.1002/2017GL076926>
- 949 Zuidema, P., Alvarez, C., Kramer, S. J., Custals, L., Izaguirre, M., Sealy, P., Prospero, J. M., &
950 Blades, E. (2019). Is Summer African Dust Arriving Earlier to Barbados? The Updated
951 Long-Term In Situ Dust Mass Concentration Time Series from Ragged Point, Barbados,
952 and Miami, Florida. *Bulletin of the American Meteorological Society*, 100(10), 1981–1986.
953 <https://doi.org/10.1175/BAMS-D-18-0083.1>
- 954